Masters Thesis
Adaptive speckle interferometry

Bence Béky

Supervisor: Dr. János Kornis
assistant professor

Department of Physics
Institute of Physics

BME
2008

Abstract

Adaptive speckle interferometry

Coherent deformation measurements, namely digitally reconstructed holographic interferometry and speckle correlation fringe analysis are studied. Their history is reviewed, theoretical foundations are summarized. Measurement layouts and data analysis are described. Desensitized arrangements and phase shift methods are analysed. Focus is on out-of-plane deformation component.

Publications in the field are reviewed with regard to adaptivity. Based on these, adaptivity is defined and possible implementations are investigated. Two characters of adaptivity are selected for detailed investigation: measurement of test objects with non-uniform illumination or reflection, and measurement of deformations being either large themselves or including large components like rotation.

Two methods are presented for adapting to non-uniform illumination. Rotation components are compensated with software and with feedback to the measurement system. Large rotations are resolved using two measurements of different sensitivite at the same time. Measurements and simulations are both presented for most of these techniques.

A new quality measure is introduced for phase shifted measurements. Its choice is justified by theoretical considerations as well as the experiments.

Results are summerized and conclusions are drawn, with focus on further improvements and industial applications.

Acknowledgements

I owe thanks to my supervisor János Kornis for his guideance, useful advice and encouragement. The outlines of this work lie on his ideas and the measurements presented here would never have been carried out without him making me familiar with every piece of laboratory equipment with infinite patience.

I would also like to mention the invaluable help of István Szilaj, the technician of our department, who developed and fabricated the PZT with its controller circuity and numerous other devices in the laboratory.

I am grateful to Balázs Gombkötő, research assistant at the department, for his various advice and `Matlab` code for Fresnel hologram reconstruction.

I would like to thank the help of Richárd Séfel, my student-mate working on his diploma thesis in the area of digital holography, for sharing me his experience with digital hologram setups and their reconstruction.

Contents

List of Figures

1 Introduction

Coherent light have been used for object shape and deformation measurement since the invention and spread of lasers. The experiments described in this work involve the concept of speckles and hologram, both requiring coherent light. It was first pointed out by Leendertz et al. that the interference of two speckle fields can be used to create interference fringes corresponding to object deformation [1]. Another possibility for deformation measurement is by means of holograms. Holograms provide a way to record the complex wavefront of an object and to perform elementary operations on it by means of double exposure or using the reconstructed hologram as reference beam. Deformations can also be substracted using a special reconstruction of doubly exposured holograms as reference [2]. These were the earliest forms of speckle and holographic interferometry.

The next stage was the combination of technology used for television with custom analog circuity to calculate correlation of speckle images to obtain the fringes. This is commoly referred to as TV holography. First Løkberg et al. studied vibrational modes in 1981 while pointing out the possible usefulness of static image deformation measurement in nondestructive testing [3]. The idea is that a structural fault shows as a local perturbance in the deformation pattern if the object is deformed under slight load. Still in that decade, deformation difference between two macroscopically identical objects was measured and examples of difference patterns due to defects were shown [4] [5] [6].

Later on, the increasing popularity of computers and availability of commercial digital cameras revolutionized both techniques. Speckle correlation images were calculated by substraction and holograms reconstructed by Fourier transformation, Monte–Carlo methods or convolution. Experimental arrangements for measuring in-plane, out-of-plane deformation and deformation gradient were elaborated [16] [17].

This work exploits these digital methods and presents a few enhancements to them. The concept is to concieve, develop and implement adaptivity of speckle interferometry deformation measurements towards as many of the experiment circumstances as possible.

Section 2 is the translation of the thesis plan specifying the tasks. Section 3 gives an overview of the theory behind the methods used throughout this work. Section 4 describes the work environment and specifies the hardware and softwave used for the experiments and simulations. Section 5 explores aspects of adaptivity and possible implementations by reviewing and discussing publications in the field.

Section 6 presents two independent methods used for speckle interferometry of an object with uneven reflection or uneven illumination: here adaptivity towards object intensity is shown. Section 7 studies deformation components and how they can be separated after the measurement is carried out, during the processing of data. Section 8 presents a measurement setup for deformation component separation: these are examples of adaptivity towards large

deformation components like rotation. Section 9 combines speckle pattern interference with digital holography to extend measurement range: this means adaptivity towards large deformations. For most of these measurement techniques, simulation is presented and studied along with the experiments carried out in real life.

Section 10 analyses the use of variance as a quality measure for fringe information content and finally section 11 briefly summarizes the results and inferences.

2 Task list

- Publications on adaptive optical measurement techniques are reviewed and summarized. Their feasibility in speckle interferometry and digital holography is investigated.
- A procedure for measurement of a surface with uneven reflection is elaborated. Its features are presented in simulation and measurement as well.
- Resolving interference fringe systems due to composed deformations to their components is investigated. Examples are presented in simulation and measurement as well.
- A measurement layout is proposed for separating deformation components. Measurements are carried out on this setup.
- A measurement procedure is elaborated for large deformations in such a manner that the measurement system is capable of controlling the measurement sensitivity. Its features are presented in simulation and measurement as well.
- Quality measures are proposed as an aid for the processing and analysis of interference images.

3 Theoretical background

3.1 Speckles

Objects illuminated by coherent light feature a characteristic phenomenon: their surface appears to have a granulated structure. These grains are called speckles. Speckles observed form in our eye or the imaging optics of the camera: one point of the focused surface is the source of light, to which many different paths are offered to the corresponding nerves on our retina or pixel of the camera. These paths generally vary much more than the wavelength, resulting in a uniform distribution in phase. These are then summed coherently to provide independent normal distributions for the real and complex part of the wave amplitude, giving rise to negative exponential distribution of its absolute value.

The speckle size depends on how much these random path lengths are correlated between neighboring points on the surface, as well as the variety of paths allowed, that is, size of the aperture. It is interesting to note that moving our head sideways causes the speckles to move parallelly, in the corresponding direction if we focus behind the object, and in the reverse direction if we focus in front of it. This is made use of to diagnose myopia and hyperopya.

This speckle phenomenon explained, created by the observing system, is called subjective speckle field, as opposed to objective speckle field, result of coherent diffraction on some object. Objective speckle field exists in space without being observed, in fact, it cannot be observed remotely but by placing a naked CCD at the spot in question. [16]

3.2 Speckle interferometry

Subjective speckle pattern is determined by the surface. In fact, as speckle intensity is determined by distribution of different path lengths light can take from the given surface point to the observing nerve or pixel, it changes little if this distribution is maintained. Moving the source towards the observer changes these paths and thus causes phase shift. This change is proportional to the displacement in the first order approximation with respect to aperture diameter/object distance ratio. Percieved phase changes according to total path length change, proportional to object deformation. In-plane displacement component also influences phase change while preserving overall speckle pattern, however, the pattern is shifted accordingly, possibly complicating image processing.

Interference speckle patterns are due to dual illumination of the object or coupling a reference wavefront in the field of view of the camera with a beamsplitter. Figure 3.1 shows a most simple measurement layout. Speckle patterns are assumed not to change but in phase due to deformation, hence correlation of camera captures before and after deformation shows interference fringes. Correlation is most easily revealed by forming the absolute value of the pixelwise amplitude difference. Phase changes of even multiples of π results in zero values while odd multiples in values with highest expectance on the difference image, with inevitable speckle nature.

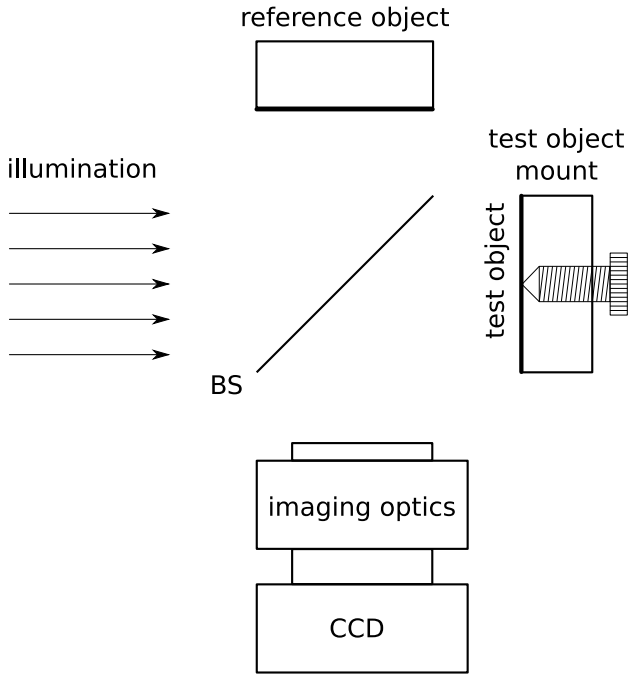

Figure 3.1: Speckle interferometry setup

3.3 Digital holography

Digital holography is a method of reconstructing complex wavefronts from single or multiple images recorded with a camera without any imaging optics. That is, the recorded intensity distribution, or in other terms, an intersection of the objective speckle field, is the

interference of the object wave and the reference wave. The reference can be a spherical wavefront originating at any distance, or as a special case, can be planar as well. A very simple holographic measurement schematic is presented in Figure 3.2.

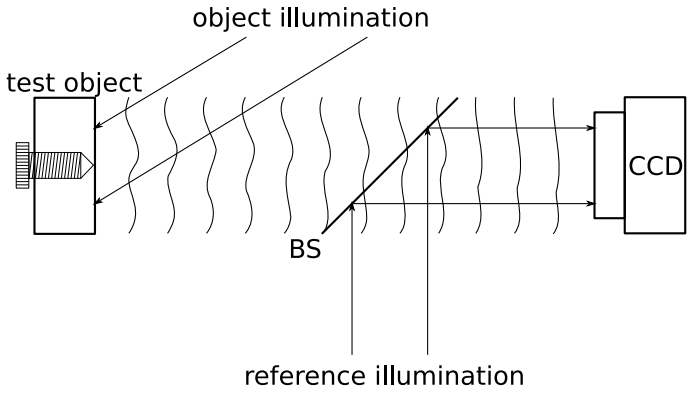

Figure 3.2: Holographic measurement layout

Hologram reconstruction has as input parameter not only the distance of the reference point source or the knowledge of the reference being planar, but also the object distance. The wavefront is reconstructed principally at that distance. However, as an artifact, not only the object wavefront is present (also referred to as first order), but a bright zeroth order in the direction of the reference and a negative first order also appear. Figure 3.3 presents this scenario. These can be diminished by different ways, one of them being the HRO method, based on recording not only the hologram, but the reference and the object wave intensity distributions separately as well, hence the name. These methods are not investigated here as there is enough field of view to separate spatially the first order from the others. [7]

Holographic interferometry in the simplest case consists of adding up the captured intensity distributions and reconstructing the resulting raw image to obtain interference fringes as shown in Figure 3.4.

In the experiments presented here planar reference wavefront is used and Fresnel approximation is applied to reconstruct the holograms. More details on this method and on digital holography in general can be found in [17].

3.4 Desensitization

If interference fringes are too dense, as in the case presented in Figure 3.4, need emerges to decrease measurement sensitivity. Consider the case when the object is illuminated at angle θ to surface normal and observed from a perpendicular direction. Suppose two captures are taken: one before and one after deformation. Our goal is to determine the change in the optical path length of the beam reflected from a given point on the object's surface. Denote the in-plane deformation of this point in the plane of the illumination direction and the surface normal by Δx, the in-plane deformation perpendicular to this direction by Δy and the out-of-plane deformation by Δz (see Figure 3.5). During our measurement analysis methods it is always assumed that Δx and Δy are small enough with respect to the subjective speckle size so that they do not cause significant speckle decorrelation. This usually limits maximum detectable out-of-plane deformation to the order of 50 μm for our test object and setup.

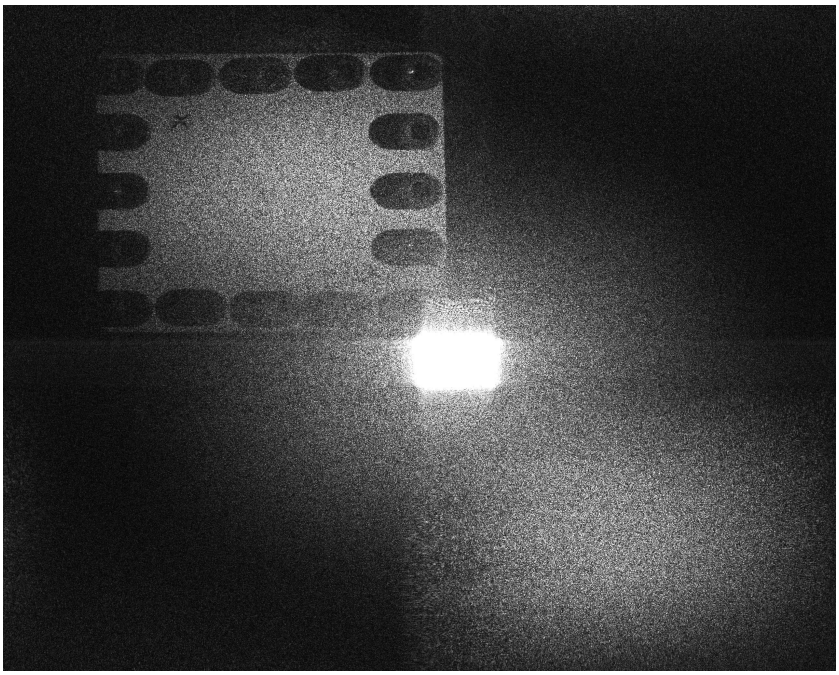

Figure 3.3: Hologram of the test object

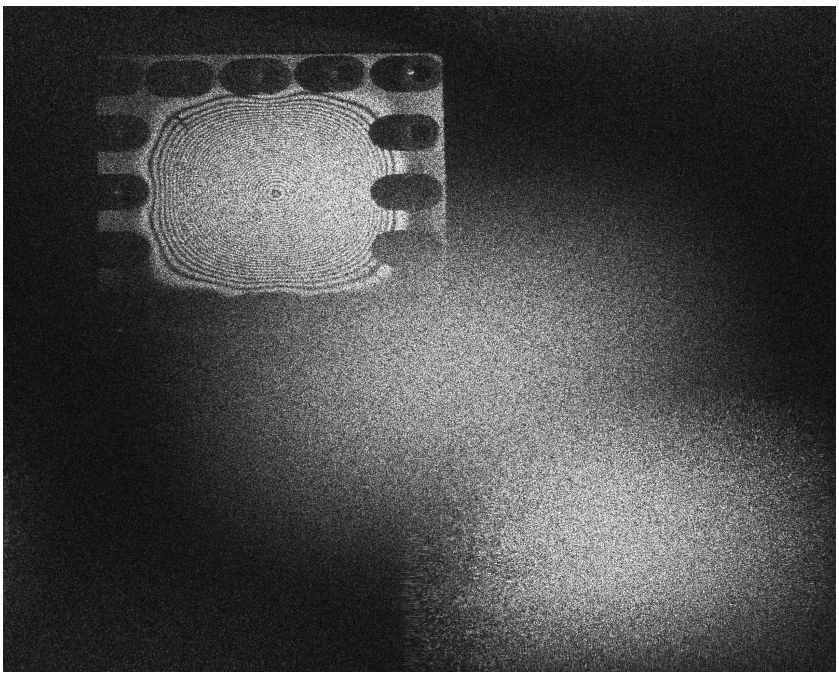

Figure 3.4: Holographic interferogram of the test object

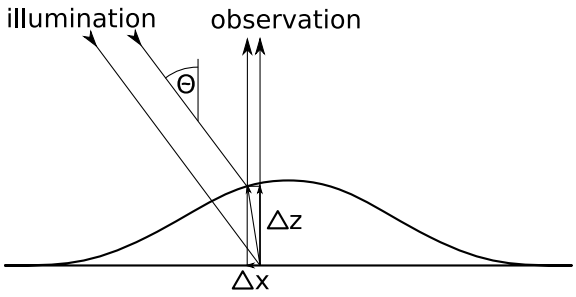

Figure 3.5: Path length change due to displacement

The optical path length will change by $\sin\theta\Delta x + (\cos\theta + 1)\Delta z$. Δy will not have a contribution as it is perpendicular to both the incoming and the outgoing beam direction. It is not shown in the figure for clarity, it is perpendicular to the plane of the figure.

This calculation applies both to speckle interferometry and digital holography. In an arrangement with reference illumination, the phase shift $\Delta\varphi$ is determined by

$$\Delta\varphi = \frac{2\pi}{\lambda}\left(\sin\theta\Delta x + (\cos\theta + 1)\Delta z\right) \tag{3.1}$$

In case of illumination perpendicular to the object, $\theta = 0°$ and

$$\Delta\varphi = \frac{4\pi}{\lambda}\Delta z. \tag{3.2}$$

It is possible, however, to create a speckle interferometry arrangement in which there is no reference object but the test object has two illuminations at angles θ_1 and θ_2. In this case, it is the difference of the changes of the optical path lengths of the two beams that determines the correlation between the captures before and after deformation. This means that

$$\Delta\varphi = \frac{2\pi}{\lambda}\left((\sin\theta_1 - \sin\theta_2)\Delta x + (\cos\theta_1 - \cos\theta_2)\Delta z\right). \tag{3.3}$$

Δx is omitted from now on as in-plane deformation of metal plates is usually much smaller than out-of-plane one, and $|\cos\theta_1 - \cos\theta_2|$ is referred to as desensitization factor.

This argument can easily be generalized to the case when the test object is not observed from a perpendicular direction but from an other given angle. It is easy to see that in the desensitized case this makes no difference as both illuminations travel the same distance from the surface to the observer. [16]

3.5 Phase shift methods

There are various phase shift processing algorithms as described in [18]. Our research group has previously used the three-frame and four-frame methods. The idea is to have three or four correlation images with $\frac{\pi}{2}$ increment in the relative phase shift between successive captures. That is, a master reference image is taken before deformation, and three or four images are captured after deformation, with increasing phase shift introduced in one of the two interfering wavefronts. Then three or four correlation images are calculated, each by forming the absolute value of the difference of one capture corresponding to a certain phase shift and the master capture. Then it is possible to calculate $\Delta\varphi$ due to deformation based on these three of four values pixelwise.

Clearly it is equally possible to record four images before deformation and one after, and circumstances determine if one method is favourable to the other. It is important to note, however, that deformations cannot be reproduced, which limits measurement methods in a way that all image capture circumstances (ie. illumination, camera lens setting, aperture size) has to be reproducable except a single one. Examples are provided for such complicated expermiental scenarios in Sections 6 and 9.

The measurements presented here are processed by a more advanced method known as Carré technique. This has the advantage that it does not rely on the actual amplitude of the phase shift increments, only on them being equal. This is of great help if the PZT coefficient is not known, only its linearity is assumed. Clearly, 0 or 2π phase shifts do not carry information, similarity, too small phase shifts or those too close to multiples of π are likely to have a large error. Thus an amount close to $\frac{\pi}{2}$ was selected.

In fact, this technique has the additional advantage that it also works if the phase shift is not constant throughout the object, as long as it remains linear. This might be the case with non-planar illumination wavefronts.

Let α denote the phase shift between consecutive captures, $\Delta\varphi$ the phase difference change between the interfering wavefronts due to deformation at a given pixel, and I_1, I_2, I_3 and I_4 the intensity values for that pixel respectively. Then Carré's method tells us that

$$\tan\frac{\alpha}{2} = \sqrt{\frac{3(I_2 - I_3) + I_4 - I_1}{I_1 + I_2 - I_3 - I_4}}, \tag{3.4}$$

$$\tan\Delta\varphi = \tan\frac{\alpha}{2} \cdot \frac{I_1 + I_2 - I_3 - I_4}{I_2 + I_3 - I_1 - I_4}. \tag{3.5}$$

However, care should be exercised when substituting (3.4) into (3.5) and calculating $\Delta\varphi$ directly. There is a careless simplification in [18] which fails as

$$\sqrt{\frac{3(I_2 - I_3) + I_4 - I_1}{I_1 + I_2 - I_3 - I_4}} \cdot \frac{I_1 + I_2 - I_3 - I_4}{I_2 + I_3 - I_1 - I_4} \neq \frac{\sqrt{(3(I_2 - I_3) + I_4 - I_1)(I_1 + I_2 - I_3 - I_4)}}{I_2 + I_3 - I_1 - I_4}$$

in general, depending on the sign of $I_1 + I_2 - I_3 - I_4$.

In fact, feeding the two parameters

$$\tan\frac{\alpha}{2} \cdot (I_1 + I_2 - I_3 - I_4), \quad I_2 + I_3 - I_1 - I_4 \tag{3.6}$$

into a four-quadrant inverse tangent function, called `atan2` in most programming languages, returns the correct value for $\Delta\varphi$ modulo 2π. [18]

As no active phase shift feedback is implemented in any of the measurement setups described here, random phase shifts occured due to air circulation and mechanical vibrations in the laboratory. It is therefore important to note that methods exists for calculating path length change in case phase shift is not known. One such method is described in [8].

4 Technical details

This section describes the general circumstances determining the activity presented here. An overview is given on the devices used for the experiments, the experiment setups are briefly described and the software tools used for simulations and measurement data analysis are presented.

4.1 Experimental devices

A Spectra-Physics Lasers manufactured Model 127 50 mW He-Ne laser is used as a coherent light source in our experiments. It features a wavelength of 632.8 nm and a coherence length in the order of a few centimeters.

Phase shift is introduced by a piezoelectric crystal driven by a AD7391 10 bit serial input DAC and a high voltage op-amp fed by a DC-DC converter. The maximum output voltage is 380 V. The DAC is interfaced to the parallel port of a PC via 74HC14N Schmitt-triggers.

The camera used in our experiments is a model MX13 by Baumer Optronic. It has a CCD with resolution of 1280×1024 and 8 bit depth.

As test objects, bronze diaphragms of size 40 mm by 40 mm and thickness 0.25 mm are used, painted white. They are fixed to a holder by 16 screws and can be loaded in their center via a micrometer screw.

4.2 Experiment setups

Throughout this work, out-of-plane deformations of test objects are measured. So the experimental setups feaure at least one beamsplitter and beam expanders for each beam to provide uniform illuminations. Deformation dependent speckle pattern is generated by either interference of the test object wavefront with a reference wavefront or by directing two illuminations to the test object at different angles. The latter introduces a desensitization as described above.

In both cases, test object is focused on by the camera. This is done in incoherent light since subjective speckle pattern is always of the same structure, even if unfocused, so a laser-illuminated object is difficult to focus on. When using reference wavefront, it originates from diffuse reflection from another illuminated object, which however does not have to be focused on.

To obtain not only an interference fringe pattern but information about the deformation amplitude (wrapped, that is, modulo half wavelength or so, see Equation (3.2)), speckle patterns are recorded with various phase shifts. To control this, a piezoelectric transducer-mounted mirror (PZT) is introduced in one beampath before it is collimated.

4.3 Software

The camera is only supported under the Windows 2000 operating system. Captures can be taken with the utility Optronic 2.4 and saved in bitmap files.

The PZT is controlled from a simple application I have developed in C++ Builder.

All measurement analysis, simulation, images and graphs are done in Matlab R14 7.1.0.

4.4 Measurement analysis methods

The first step in image processing for out-of-plane deformation speckle measurement is the calculation of correlation images by forming the absolute value of the pointwise difference of the two captures. Change of optical path lengths of interfering wavefronts resulting in speckle decorrelation is a phenomenon having roots in the nature of speckles, thus it is the correlation of the speckled images that has to be calculated. However, speckles on interference fringes are not wanted as fringes themselves are of our primary interest. These are areas of different intensities by nature, disturbed by the speckle pattern. Therefore to process fringes, taking into consideration phase shift or not, speckles have to be averaged over. This is carried out by a low-pass filter, namely convolution with a Gaussaian kernel. This implies that

speckle size has to be considerably less then fringe spacing so that it is possible to get rid of speckles without reducing fringe contrast. Fringe spacing should be at least five times speckle correlation length. [16]

4.5 Unwrapping

The obtained phase values are modulo 2π, or in other words, wrapped. Individual pixels do not bear more information about the magnitude of the deformation. There are many possible approaches to reconstruct this information. For instance, deformation can be recorded in many small steps between which there is no pixelwise phase shift larger than π so that it can be tracked.

A more widely used solution is to unwrap the phasemap. This is done in principle by finding the edges of 2π jumps and shifting each area by the proper multiple of 2π, a method called integration, so that they get into alignement. However, in practice there are always singularities, that is, essential discontinuities with residues of a nonzero multiple of 2π, causing ambiguity of the integration process. Many times there is a chance to connect residues of opposite signs if they are close and avoid this connection, called cut, in the integration process. This is the basic principle of Goldstein's cut-line algorithm [9].

A `Matlab` implementation of this algorithm is available at [19], which is used with slight improvements.

5 Adaptivity

Publications on adaptive optical measurement techniques are reviewed and summarized. Their feasibility in speckle interferometry and digital holography is investigated.

5.1 Adaptivity in general

Measurement circumstances like illumination, magnitude of deformation to be examined, object size, material, surface roughness and reflection, ambient temperature and airflows can vary on a large scale from measurement to measurement. Airflows do vary air temperature and humidity in the way of the beam, changing the optical path length. The capability to accomodate to these or any other external parameter is called adaptivity. For a measurement system this feature can be implemented through analyzing incoming data via given quality measures and influencing the measurement based on the obtained information through actuators, that is, devices capable of setting illumination, focusing and zooming the camera, changing aperture size, gain and shutter time, shifting phase, moving the camera, object or illumination, and through software parameters in data processing like low-pass filter bandwidth or logical deformation compensation. This should be carried out in such a way that the optimal result is produced with respect to precision, reliability and computational resources. [10]

One brilliant example for adaptivity is controlling illumination by the computer as described in [11]. For different illuminations, areas with intensity in a predefined range are processed and these deformation maps are merged. This method is suitable for processing objects illuminated unevenly or with reflection varying in a great range. It is also possible to handle the case where the two interfering illuminations have different intensity distributions. This work further improves this method: areas are selected not based on their intensities but other measures of deformation information content as described later.

Another example of adaptivity is to separate deformation components, either via software or via feedback to the test object or deforming the reference object. This could make it possible to see certain local deformations due to structural faults. Examples for this are also presented in [11] and this method is further developed in this work.

Further adaptivity towards these and other circumstances is discussed at the end of each section.

5.2 Active measurement

The concept of active feedback loop is also studied and its importance is discussed. An active feedback keeps track of eventual relative phase shifts of the two illumination wavefronts by means of splitting both beams and constructing a separate interferometer, and compensates them real-time by a PZT in one beampath. These unwanted phase shifts are due to airflows, mechanical vibrations or instability of the optical components. It is important to note that interferometer design should focus on being as closely coupled to the object deformation measuring interferometer as possible, since any additional optical element introduced or additional beampath through air causes deviations in relative phase shift decreasing the efficiency of the method.

The feedback can be implemented in various ways. It is possible to use a detector line with every fourth cell connected to detect the position of a parallel interference fringe system of matching period. A 3 kHz probe signal of small amplitude is added to the PZT driving signal and the detector output is analysed with a lock-in amplifier. Phase shifts of multiples of $\frac{\pi}{2}$ can be obtained by using different outputs of the detector [12].

It is enough to use a single detector pixel for lock-in input. Phase shifts of multiples of $\frac{\pi}{2}$ can be easily obtained by using derivatives of different order of the detector signal [13].

Another approach is to use photorefractive crystals as feedback. This stabilizes phase regulation on a small timescale, however, drift appears on the scale of few seconds [14].

It is described in all three articles that a high stability is achieved against mechanical vibrations of the optical table or individual optical elements, or convection introduced by intense heating or by means of a vent. These methods are nowadays widespread to stabilize phase shift, however, the measurements described here do not implement them. This results in the measurements needing to be carried out many times to obtain results not suffering from unevenly shifted phases, which would of course not be acceptable in an industrial environment.

6 Uneven reflection

A procedure for measurement of a surface with uneven reflection is elaborated. Its features are presented in simulation and measurement as well.

6.1 Introduction

Test objects with uneven reflection can cause difficulties in speckle measurements. In arrangements without reference beampaths, i.e. desensitized ones, the dynamic range of the image capture device might not be sufficient for the whole image area to be processed – bright areas will mostly be saturated while dim ones suppressed by electronic or quantization noise. This situation requires multiple captures with different exposure times or gains so that their useful intensity ranges overlap.

In arrangements with reference beampath, in addition to the capture device dynamic range limitations, the ratio of object and reference intensity must lie within a specific range to result in fringe patterns with sufficient contrast. This range is smaller than the camera range to noise ratio, since with the given exposure and gain settings, the intensity resulting from the sum and the difference of object and reference wave amplitudes must both not be oversaturated or dominated by noise.

If the reflection of the test object varies over a great range, this necessitates multiple image captures with different reference intensities. Exposure times should also be adjusted in such a manner that the overlap between image area of optimal illumination/reference intensity ratio and that of optimal captured intensity range is maximal.

In both situations, images need to be captured before and after deformation in corresponding sets, under the same circumstances, that is, illumination and reference intensities and exposure times. Then there are different approaches as how to merge information of these images.

One is to process interference fringes and deformation phase for each set of captures, then select for each pixel or small area the set with most accurate result based on some quality measure, and compose the entire deformation map from these. This method will be referred to as processing of separate recordings.

Each set of five captures should give the same deformation map with some areas being useful and others suffering from noise. The key is that different scenarios result in different areas being useful and these can be combined straight. However, during manual modification of measurement parameters, such as illumination intensity, some additional phase shift is possibly accidentally introduced to some of the beam paths, resulting in a virtual constant deformation. Therefore there might be need to adjust the deformation maps of different areas at their boundaries with a compensating constant shift. This artifact loses some information about the deformation, however, its overall shape is preserved. This kind of error can barely be avoided as adjusting a filter in the setup involves enough movement of air around the optical table for this shift to appear. However, it can be eliminated by using only electronically controlled devices to adjust intensities, thus avoiding human motion around the experiment setup.

Another approach is to merge images of different, known exposure times taken within otherwise identical circumstances to get superimages of increased dynamic range. These can be used afterwards to get an interference fringe pattern and deformation map. This method will be referred to as dynamic range extension. It can only be applied if reference intensity does not have to be adjusted, which practically means desensitized measurements: in a conventional arrangement, if the test object reflection varies more that the camera dynamic range could handle, it would also make it necessary to change illumination ratio so that this method could not be used.

As camera exposure time is set electronically, unwanted phase shifts are less likely to occur during these measurements in which no other parameter is adjusted.

The idea for this experiment has been suggested by [11], but here phase shift is applied and thus different measure is used for fringe contrast.

6.2 Simulation with processing of recordings separately

In this subsection, a test object with uneven reflection is investigated via simulation. The arrangement is presented in Figure 6.1. The test object of resolution 256×256 pixels has an exponential reflection dependence along the x-direction through a range of $1 : e^{20}$. 20 different exposure times are used according to a geometrical sequence. This results in 100 recorded images in total.

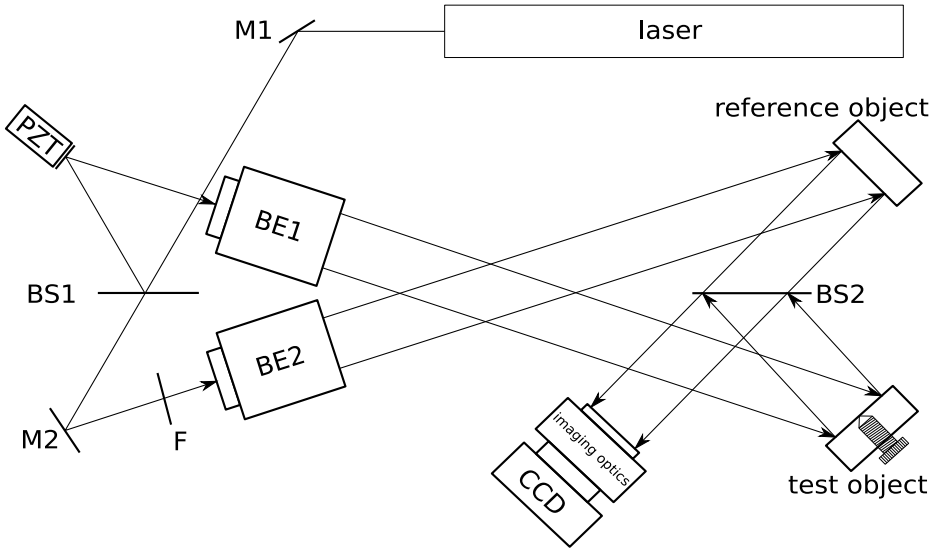

Figure 6.1: Measurement layout
Beamsplitter BS1 divides object and reference illumination. Filter F controls reference intensity. Beamsplitter BS2 merges object and reference wavefronts.

The illumination angle is $\theta = 15°$. The deformation applied to the test object has Gaussian shape and an amplitude of $d_{\max} = 1.6$ μm, resulting in $\frac{d_{\max}}{\lambda}(1 + \cos\theta) = 4.97$ interference fringes, see Equation (3.1).

The simulated camera has 8 bit resolution, and a Poisson noise of expected value of 20 is added. Pixel values higher than 255 are saturated.

The illumination of the reference is adjusted in inverse proportion to the exposure time to ensure that the area within the useful range of the camera sensitivity (that is, not saturated, nor dominated by noise) overlap with the one with optimal object/reference illumination ratio. This results in the reference being of constant intensity on the exposures. A typical exposure is shown in Figure 6.2.

Standard deviation of the four phase-shifted captures is calculated for each pixel. The result is low-pass filtered and then the exposure setting resulting in the highest standard deviation is selected for each pixel. The boundaries between the areas corresponding to the exposure setups is shown in Figure 6.3 (with a thin border for clarity).

For each exposure setting, four interference fringe images are formed by substraction of corresponding images before and after deformation, then these correlation images are low-pass filtered to average over speckles. This has to be done for the whole image as smoothing is not a point operation, even if only a small area of this fringe pattern will be used. Such a fringe pattern is shown in Figure 6.4. One the right of the visible fringes noise is present, however, on the left most pixels are saturated, hence noise does not appear.

To demonstrate the range of illumination ratio our methods can process, a phasemap calculated from this single exposure is seen in Figure 6.5. The object wavefront is too dim on the right side of the image compared to the constant distribution of the reference wave, and the left side is saturated again.

Now for each pixel, the corresponding values are selected from the four smoothed fringe

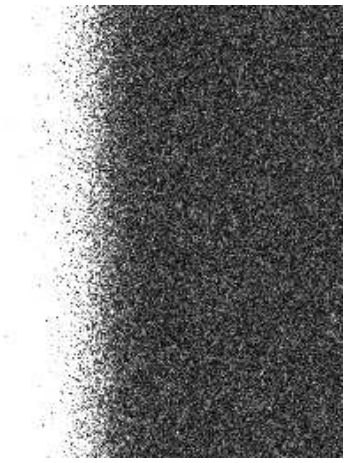

Figure 6.2: A typical exposure of the object

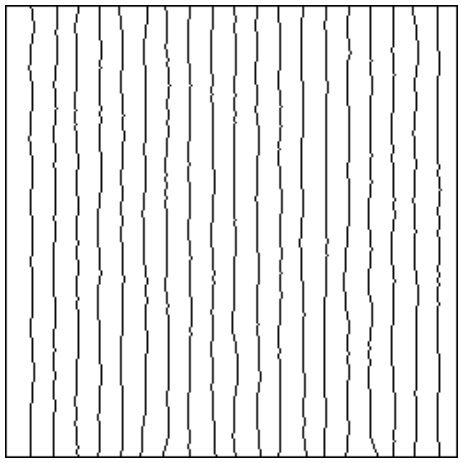

Figure 6.3: Mask boundaries based on the proposed quality measure

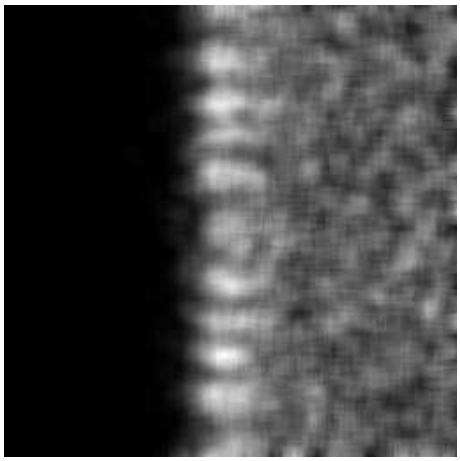

Figure 6.4: Fringe pattern from a single exposure

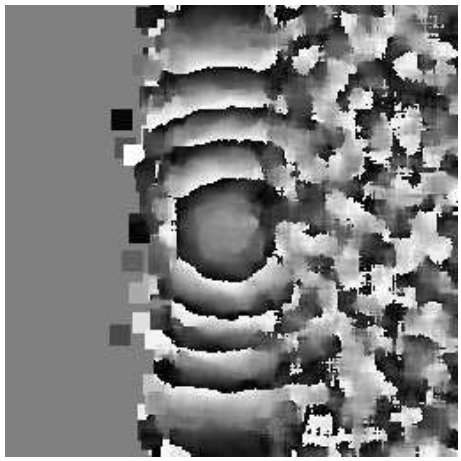

Figure 6.5: Phasemap from the same single exposure

images for which the deviation proved to be the largest as described above. Four combined images are formed, one for each phase shift, and Carré's method is applied to these. The result is presented in Figure 6.6.

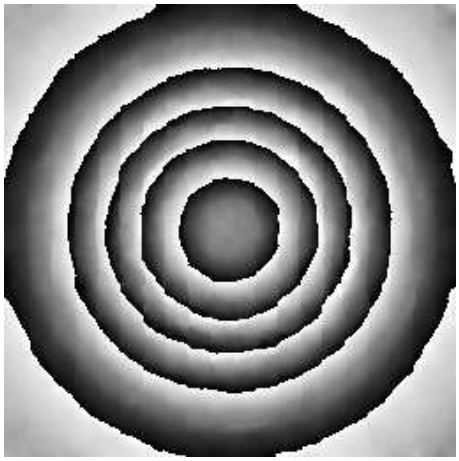

Figure 6.6: Composed phasemap from all exposures

Finally, Goldstein's algorithm is applied and the deformation map is depicted in 3D in Figure 6.7.

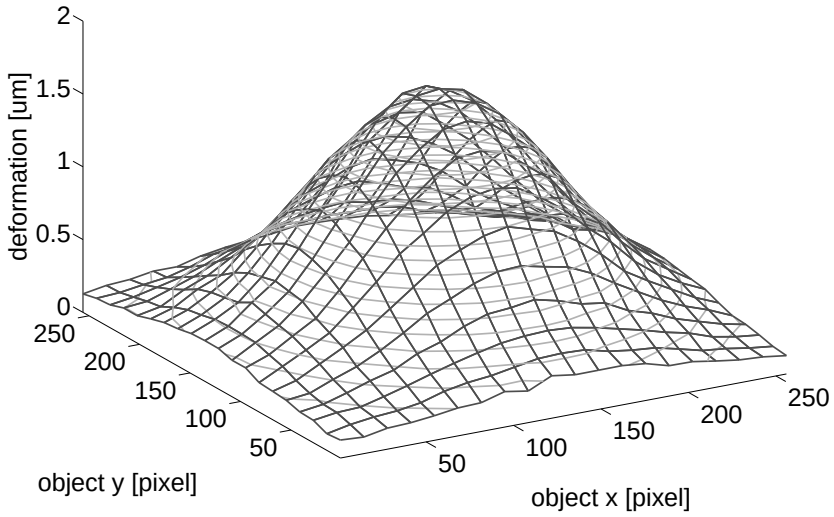

Figure 6.7: Deformation map

6.3 Measurement with processing of recordings separately

In this subsection, a test object is investigated in a measurement with the same arrangement as in the previous subsection, shown in Figure 6.1. The aim is to provide a method for measurement of objects bearing very high variations in their apparent intensity possibly due to variations in reflection coefficient or being illuminated by a wavefront being spherical or of any other shape and possibly very uneven. This is likely to happen with large object within industrial circumstances where there is no possibility to create a large planar wavefront of uniform intensity.

As black and white paints can only have a reflection coefficient ratio up to approximately 30, a diaphragm painted half black, half white, illuminated evenly is always possible to measure with ESPI, unless exposure is set deliberately to saturate most of the white area or noise is added. To demonstrate the ability of measuring objects with much wider intensity ranges, a white diaphragm is studied with uneven illumination created by inserting a filter into half of the otherwise uniform illuminating wavefront. This creates two well-separated areas. The reference illumination and exposure time are adjusted for the two areas separately so that fringe contrast is optimal. The test object illumination angle is $\theta = 15°$, this is taken into consideration according to Equation (3.1).

Reference wave illumination adjustment with manual analog devices is not precisely reproducible. Even inserting another filter in the beampath gives slightly different results each time, as its extinction depends on the area used and on the angle. The workaround for this problem is to capture an image first without the additional filter in the reference beampath, then introduce that filter, increase the exposure time and take another capture. Then the deformation is carried out and the four captures for each illumination setup are taken in reverse order, that is, four with the filter and four after removing it. This eliminates the need to insert the filter in the beampath twice. Clearly the exposures without filtering the reference are previously adjusted to give decent results on the brighter area of the object while the filter is tuned to match the dimmer area, a procedure that can be carried out adaptively, by software, in a computer-controlled environment.

Figure 6.8 gives an idea about the test object with half of its area illuminated optimally, the other half being saturated.

Correlation images are formed as usual, one of them for both illumination circumstances is presented in Figure 6.9. From four such images, deformation phasemaps can be calculated using Carré's method, see Figure 6.10. An image area is selected free from screws, so that deformation can be focused on.

Now we need to select one of the results for each pixel based on some quality measure. The pixelwise standard deviation of the four fringe patterns is used once again, after necessary low-pass filtering is applied to average over speckles. Figure 6.11 shows this quality measure for the two illuminations. The maximum value is 0.19 times the maximum pixel value of the correlation fringes.

These values are now compared pixelwise. The resulting mask (with a thin border added for clarity) is presented in Figure 6.12. Now the phasemaps from the two scenarios can be combined, as shown in Figure 6.13.

As mentioned earlier, in real experiments the two scenarios may suffer from a relative phase shift due to some accidental movement of some optical parts. This can be compensated by introducing a difference measure: the square sum of the differences of calculated phase values at the boundary points, taking into consideration 2π-modularity. Figure 6.14 presents such a difference measure as a function of the relative phase shift introduced for compensation. Then the minimum value can be selected to align the two phasemaps, as seen in Figure 6.15. It can be seen that this method has compensated for the accidental phase shift very well.

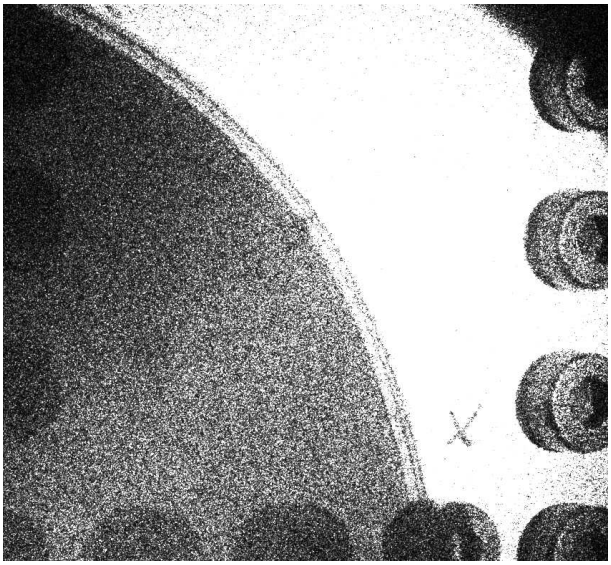

Figure 6.8: A typical capture

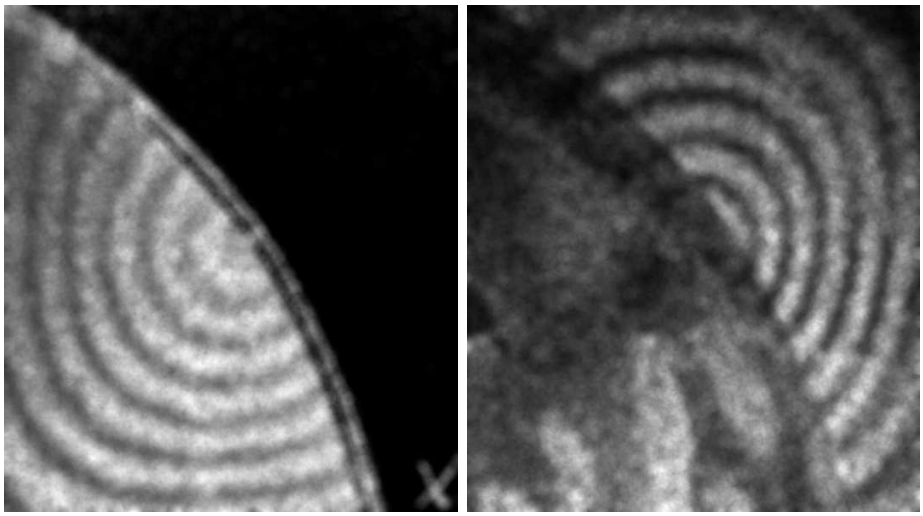

Figure 6.9: Correlation images for the two illuminations

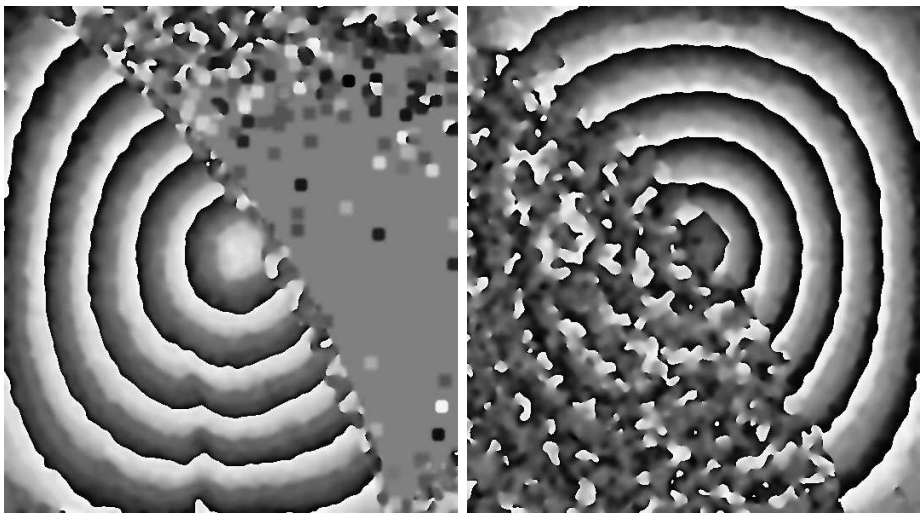

Figure 6.10: Deformation phasemaps for the two illuminations

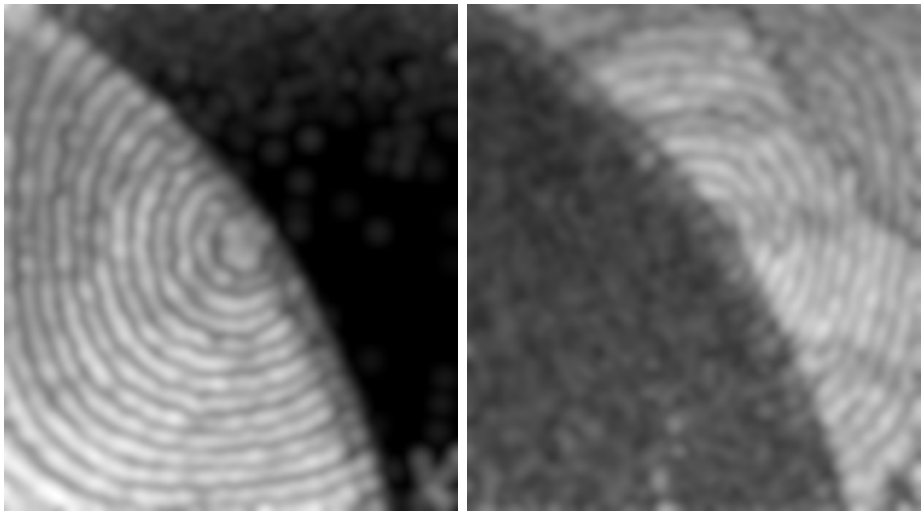

Figure 6.11: Pixelwise standard deviations for the two illuminations

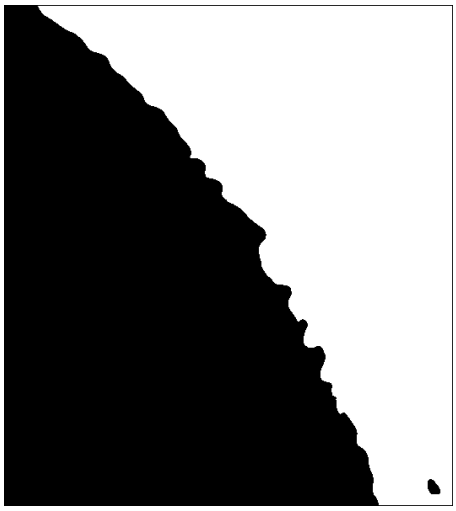

Figure 6.12: Quality mask based on proposed quality measure

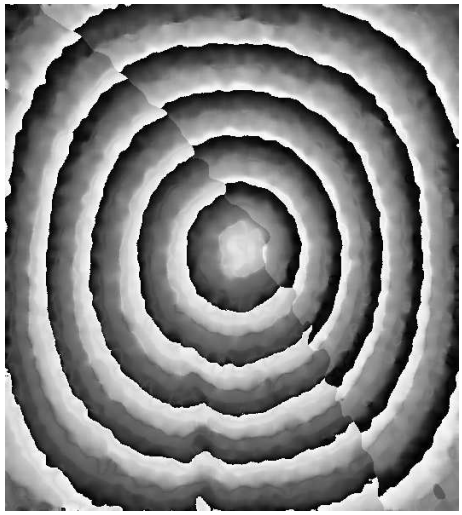

Figure 6.13: Merged phasemaps without additional alignment

Now the combined map can then be unwrapped to obtain Figure 6.16, which can be rendered in 3D as shown in Figure 6.17.

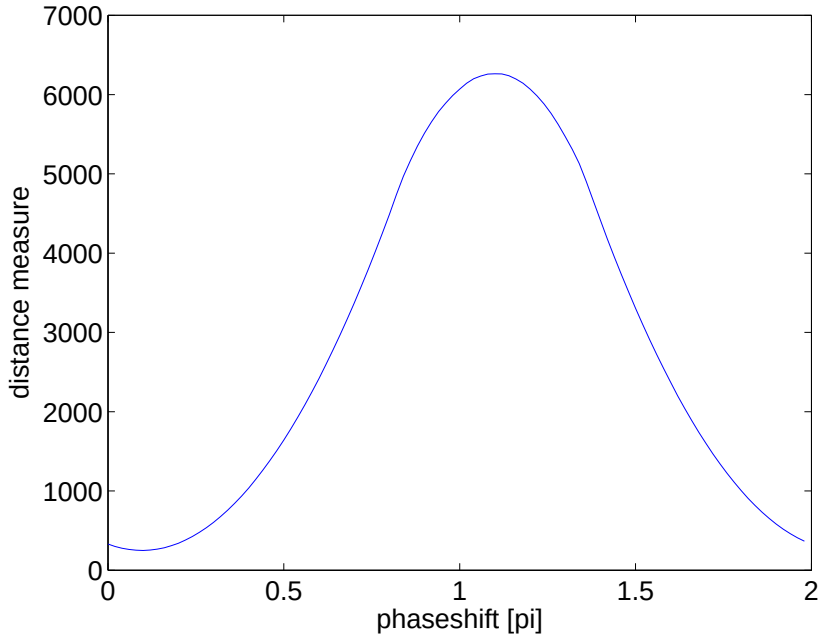

Figure 6.14: Difference measure versus relative phase shift of two phasemaps

It is clear that this method can easily be used with more that two illumination and exposure setups. The highest standard deviation can be selected likewise and also the phase

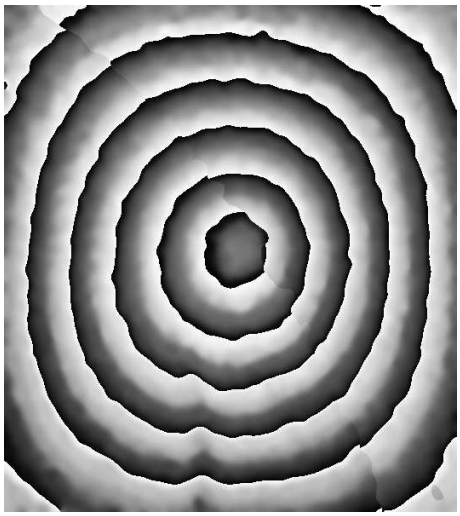

Figure 6.15: Aligned merged deformation phasemap

Figure 6.16: Unwrapped deformation map

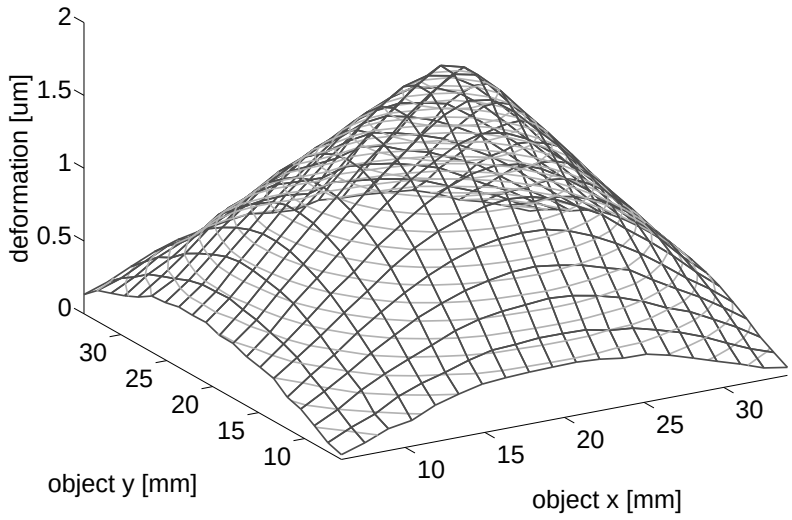

Figure 6.17: 3D deformation map

shift can be compensated either step-by-step in case only succesive exposures share boundary or by minimising in more than one variable in the general case.

6.4 Simulation with dynamic range extension

In this subsection, a simulation is carried out of a desensitized arrangement shown in Figure 6.18. The test object is of size 256×256 pixels with reflection exponentially varying in x-direction through a range of $1 : e^{20}$. The two beams shine on the object at angles $\theta_1 = 30°$ and $\theta_2 = 15°$ to surface normal and observation is from perpendicular direction, resulting in a desensitization factor of $|\cos\theta_1 - \cos\theta_2| = 0.100$ according to Equation (3.3). The object deformation has a maximum of 20 μm and is of Gaussian shape.

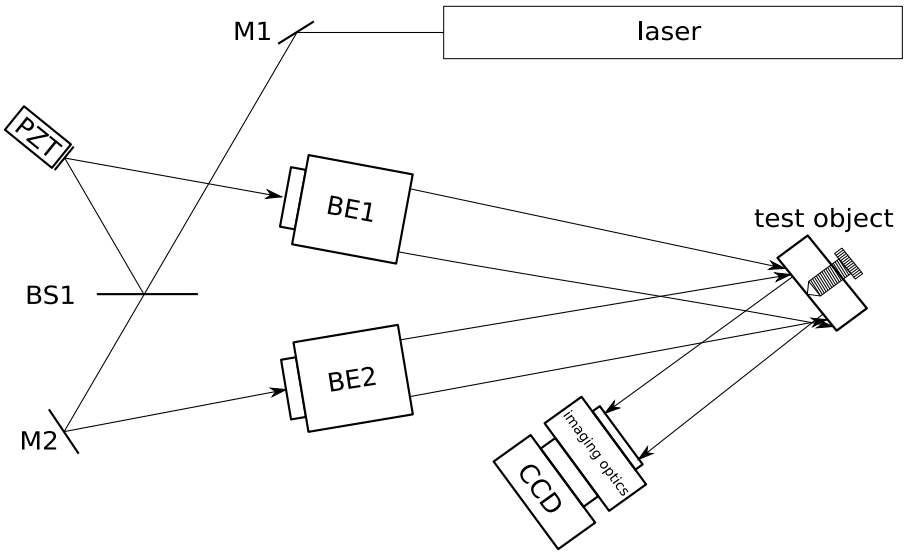

Figure 6.18: Measurement layout
Beamsplitter BS1 divides beam into beam expanders BE1 and BE2, both illuminating the object at different angles.

20 different exposure times are used, one image is recorded before and four after deformation with each of them. The images are quantized to 8 bits, that is, 256 grayscale levels, then a Poisson noise of expected value of 20 is added and resulting pixel values higher than 255 are saturated. One typical exposure is presented in Figure 6.19.

The one state before and four after deformation, each with a given phase shift between the two beampaths, are described by five physical images of extended dynamic range, all of them combined from 20 captures. These superimages feature an additional dynamic range of e^{20} which is 8.7 orders of magnitude in addition to the original range of 255, less than two and a half orders of magnitude.

In simulation any dynamic range can be achieved, however, in practice very bright pixels not only get saturated but also saturate other pixels usually in the same row in CCD cameras.

Composing the set of 20 images starts with omitting saturated pixels: these carry litte information. Then the maximum value is selected for each pixel from the raw images, this corresponds to the setting with the highest exposure time or gain with which the pixel is not saturated, giving the lowest possible quantization and electronic noise. Then the selected values are scaled according to the exposure setting known for the selected image.

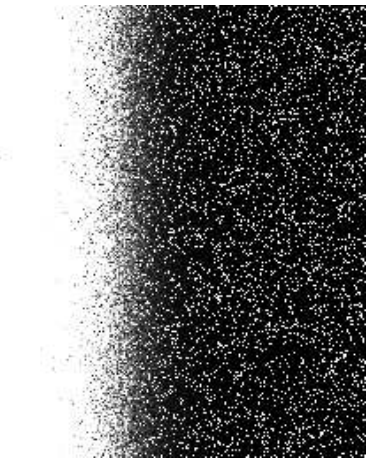

Figure 6.19: A typical exposure

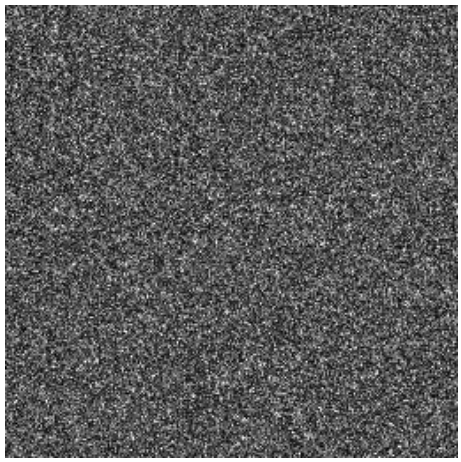

Figure 6.20: Composed speckle pattern from all exposures, with compensation

Figure 6.20 shows a composed superimage, compensated for the well-known illumination x-dependence so that all of its areas can be inspected visually. However, the spatial dependence of illumination does not have to be bothered about and no compensation is done for processing as Carré's method is invariant to scaling; it is only to reduce dynamic range to that of the printer so that we can see that the speckle pattern appears and is homogeneous apart from the varying intensity throughout the image.

Now the five superimages provide basis for four correlation images. These are smoothed with a Gaussian kernel of FWHM 6 pixels. The test object having 256 pixels across features a reflection ratio 1.08 of adjacent pixels which is low enough so that smoothing will not result in any artifact. In real measurements this ratio is usually much closer to 1.

Finally a phasemap is calculated from the correlation images, as shown in Figure 6.21. As in Subsection 6.2, a single exposure is processed and its phasemap is presented in Figure 6.22 to demonstrate that here a broader range of intensity can be processed. This is due to the deep difference that in this measurement, the interfering wavefronts both have the same spatial amplitude dependence and the speckle nature makes it possible for these values to show on a large range. The area is again limited by saturation from left and noise from right.

The phasemap from the superimages is now unwrapped and a 3D deformation map is presented in Figure 6.23.

6.5 Measurement with dynamic range extension

In this subsection a desensitized measurement is presented with $\theta_1 = 15°$ and $\theta_2 = 45°$. The measurement layout is otherwise the same as depicted in Figure 6.18. The deformation applied to the diaphragm has a peak of 3.65 μm. To emulate a test object with uneven reflection or illumination, a filter is placed right in front of the camera, thus weakening both of the two interfering wavefronts. This eliminates the need for adjustment of wavefront intensity ratio, since they appear to have equal intensities at all parts of the image. Thus captures can be taken with different exposure times and combined to superimages, which can then be used to calculate correlation patterns and finally the phasemap. The exposure times used are 10.06 ms, 36.81 ms and 107.93 ms and Figure 6.24 shows one of each respective capture.

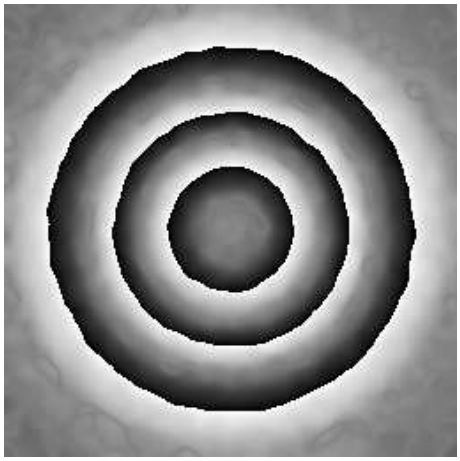

Figure 6.21: Deformation phasemap

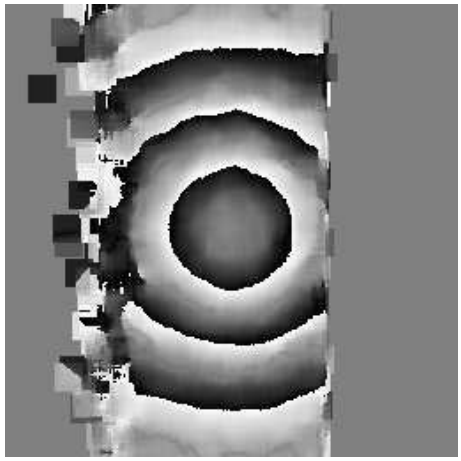

Figure 6.22: Phasemap of one exposure

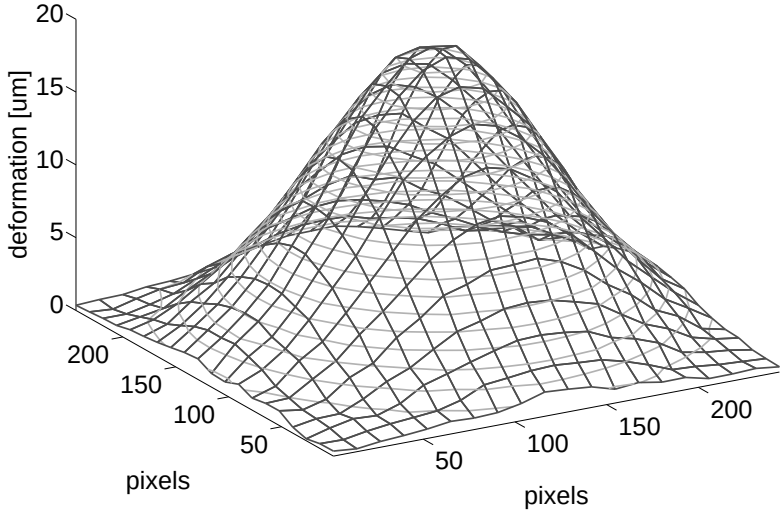

Figure 6.23: 3D deformation map

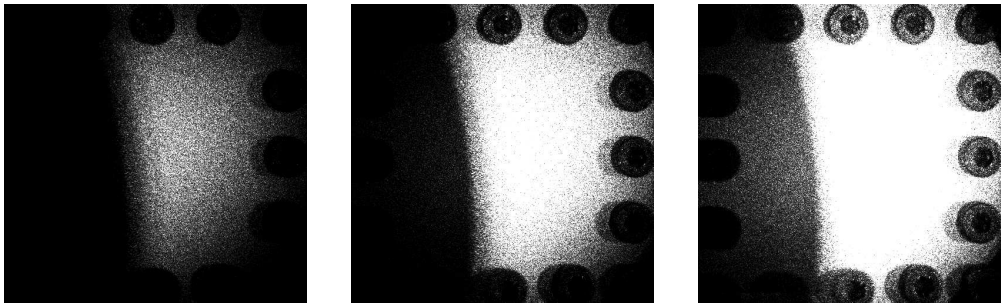

Figure 6.24: Captures with different exposure times

To demonstrate how useful these exposure settings are separately, the phasemaps calculated by Carré's technique for each exposure separately are presented in Figure 6.25.

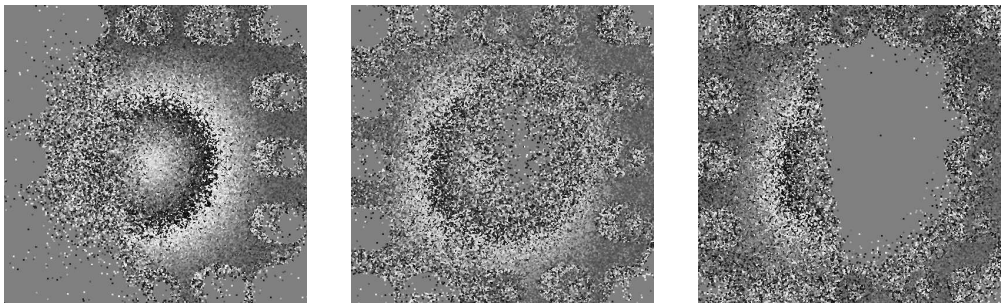

Figure 6.25: Phasemaps for different exposure times

It is seen that none of the exposure times would be appropriate to measure the whole object area. However, combining these results as explained above gives us a dynamic range covering all areas. The resulting phasemap is presented in Figure 6.26.

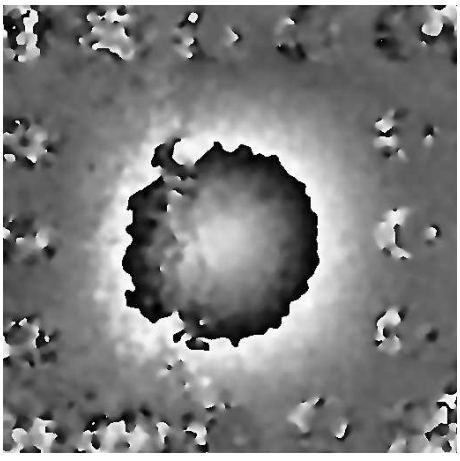

Figure 6.26: Phasemap from combined images

Finally the deformation is unwrapped and presented in 3D in Figure 6.27. It is visible that there is some wobbling near the boundary of the bright and dim areas. This is due to the unavoidable smoothing over this boundary while processing the interference fringes. However, this would not pose a problem in case there were no sharp edges in object illumination or reflection.

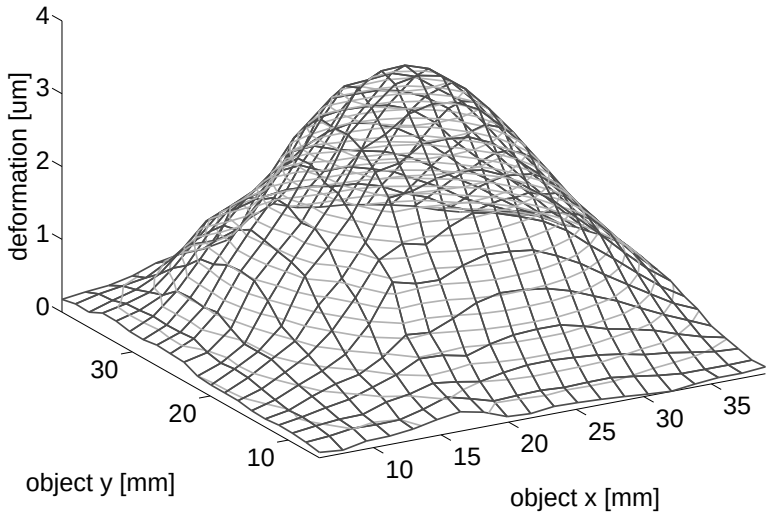

Figure 6.27: Deformation map from combined images

6.6 Conclusion

Two methods have been presented and investigated for extending the processable range of object reflection, one of them is capable of composing measurement results even if overall object illumination or reference intensity have to be changed. The simulations and experiments lead us to the following conclusions:

- Carré's method is very robust, it gives good results for a wide range of illumination and reference intensity ratio.
- Linear averaging over an area involving illuminations of slightly different magnitudes does not spoil results.
- This also means a fairly high noise tolerance if averaging is done over a sufficiently large area.
- Variance is a useful measure of fringe information content for composing measurements.
- Dynamic range extension is sensitive to sharp variations of illumination thus proves to be less favorable than separate measurement processing.

Both methods presented here do provide feedback about the quality of image areas through the measure of deviation. This information can be used to control measurement parameters, that is, refine the sequence of reference intensities and exposure times or extend their range as necessary to obtain deformation data with required precision, thus increasing the adaptivity of the method.

7 Logical resolution of interference components

Resolving interference fringe systems due to composed deformations to their components is investigated. Examples are presented in simulation and measurement as well.

7.1 Composite deformation in general

Deformation components can be classified as local or global. This distinction is extremely important in industrial applications where structural faults in cast parts result in characteristic deformation patterns locally if the object is exposed to tension. Local components can be classified based on their symmetries, however, as the aim is their detection and not their analysis here, this classification is not explained in detail.

Global deformation components can be approximated by polynomials. Concerning out-of-plane deformations, the one degree of freedom of the zeroth order term is connected to the translation of the object. The two degrees of freedom of linear deformations correspond to rotation. These might not be connected to the change of the shape but rather an overall displacement of the test object.

The three degrees of freedom of cubic components describe curvature in two directions and skew. Not being isometries, these suggest deformation of the object.

For in-plane deformation, there are twice as many degrees of freedom for each order. Here zeroth order describes lateral translation while first order corresponds to affine transformations.

Note that this distinction of local and global deformations is based on their size. However, as the area investigated can be quite limited in optical speckle interferometry, local deformations can extend beyond the borders of the image captured. In this case, the attribute local is not valid any more. In the scope of this document, a deformation is considered global if it is of degree at most three, as described above. As there is no way to tell one due to a crystal dislocation from one of high orders, all other deformations are considered to be local, and higher order global terms are neglected.

Our aim is to separate local features from the background, which is considered to result from deformations global in nature. To do so, global deformation components are approximated up to some order and substracted from the total deformation so that local features become immediately visible or recognizable by software. This can be achieved by fitting a polynomial of the desired degree on the deformation map. The local deformations are hoped not to influence this fit to such an extent that would make their recognition impossible. This is usually the case when an area large enough is investigated. In this case the method is very robust and straightforward.

Here a slightly different, however, equally important application of deformation decomposition is presented. A scenario is investigated, by means of simulation and measurement as well, where deformation gradient exceeds the processing limit of the system. However, compensation by estimated global deformation components provides a phasemap featuring gradients low enough to be processed. This section focuses on software compensation of the

deformation map while the next section introduces hardware feedback to the measurement arrangement.

7.2 Composite deformation simulation

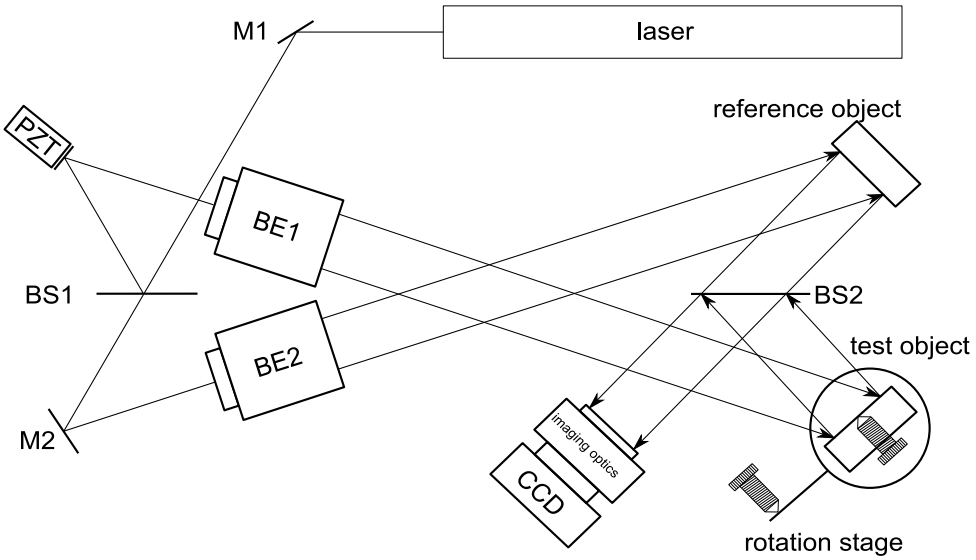

Figure 7.1: Measurement layout
Beamsplitter BS1 divides object and reference illumination. Beamsplitter BS2 merges object and reference wavefronts.

The test object is of resolution 256×256 pixels. Regular speckle interferometry setup is simulated with reference wavefront, the layout is shown in Figure 7.1. The test object illumination has an angle of 15° to surface normal, this is taken into consideration according to Equation (3.1). A circular deformation is caused by a point stress in the center, with amplitude of 3.7 μm. The wave path difference across the x-axis of the image area is of the same magnitude, due to the rotation of the test object. These add up to produce a deformation gradient too high to be processed in some parts of the area investigated.

The camera has 8 bit dynamic range and a Poisson noise of expectance 5 is added.

First, four correlation images are formed and Carré's method is applied to produce a deformation map (Figure 7.2).

The deformation map is then low-pass filtered by convolution with a Gaussian kernel of standard deviation of 5 pixels. This is necessary to remove the noise, otherwise unwrapping would be impossible at any part of the image. However, low-pass filtering with a lower cut frequency would ruin a larger area of the map. Note that experience shows that with so noisy images averaging of the deformation map gives a better result than averaging of the correlation images before applying Carré's method, as it is done in general. This is due to the fact the phase averaging preserves information better than intensity averaging of sine values of the corresponding phases thanks to the nonlinear nature of sine. As in most cases noise is not so heavy and interference fringes are more loosely spaced, Carré's method is used on a low-pass filtered correlation image as it does not handle speckles well.

It is necessary to describe averaging of phase values. These values range from zero to 2π with the curiousity that the ends of the interval are corresponded. Periodicity makes

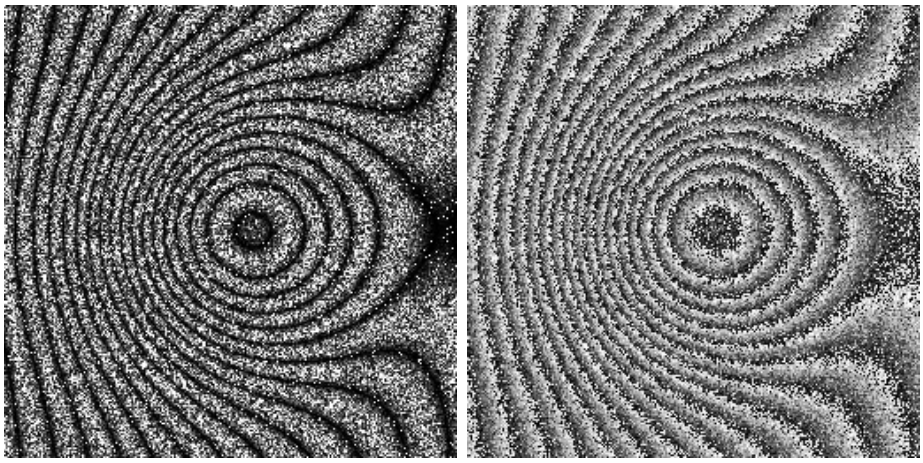

Figure 7.2: Correlation image and deformation map

choice of interval limits arbitrary as long as its length is 2π. The average or other linear function of some values within a very small range is clear: the interval has to be selected in such a way that its limit does not cut through values thought to be close to each other. In fact, this approach can be extended with ease up to the case when the phase values in question lie within an interval of length at most π. This is not likely to be the case for a single large smoothing kernel, not to mention all such areas within a 256×256 image. This would necessitate an error handling mechanism.

Instead, a much simpler approach is used: phase values are represented as complex numbers of unit magnitude with the corresponding argument. This map conserves the cyclic nature of the phase. The weighted averaging function can be used on the complex numbers in a linear fashion. Finally, the magnitude of the result is omitted and its argument is taken as the average of the phases. The case of this being undefined, that is, the complex numbers having the origin as the center of gravity can only occur if there is a symmetry of rotation, an ambiguity that could not be resolved by other means of averaging either. However, as argument (complex phase) function is defined for zero as well, no separate error handling is needed. It is easy to see that this method gives the expected result for phase values in a very small range and gives a reasonable result in any case.

Goldstein's method is used for unwrapping of the averaged phase map. The area of highest deformation gradient cannot be unwrapped, as shown in Figure 7.3. It can be seen on the low-pass filtered phasemap that these are the areas where 2π wraps become so closely spaced that even such a small kernel messes them up. 91.5% of the area is unwrapped successfully.

However, the implementation of Goldstein's method we use also tells us which areas were unwrapped properly. Hence a linear function can easily be fit to these deformation values. This component is substracted from the raw deformation map, spacing up the interference fringes. Hence the same low-pass filter removes the noise again but now does not mess up wraps (Figure 7.4). This compensated image can now be unwrapped.

The method of compensation is very easy in our case: the raw phasemap is multiplied by a complex number of argument corresponding to the compensation data. Note that a similar method has been used earlier at our department [15]. This consisted of quantizing the compensation data to $\frac{\pi}{2}$ units and cyclically perturbating the four $\frac{\pi}{2}$ phase shifted fringe patterns accoringly. This is an innovative method in case a single compensated fringe pat-

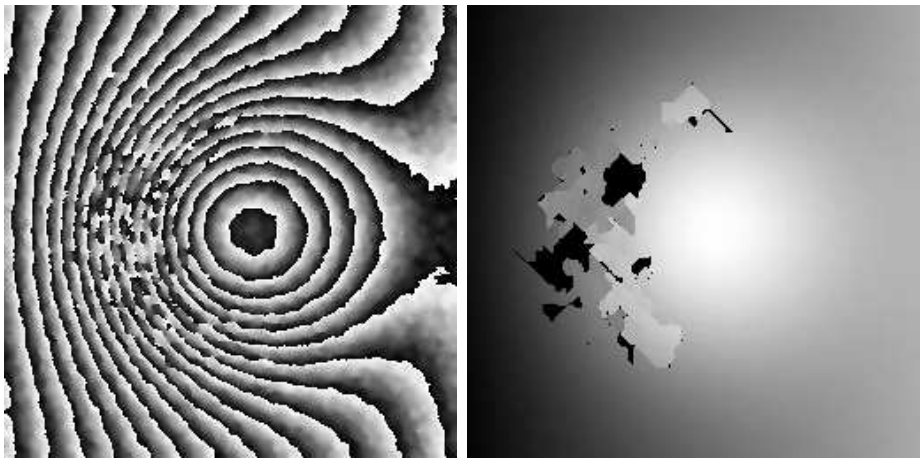

Figure 7.3: Smooth deformation map and its unwrap

tern is needed. However, carrying out any phase calculation method on the perturbated fringes results in a quantized compensation, therefore it would be no better than the method described here for our purposes.

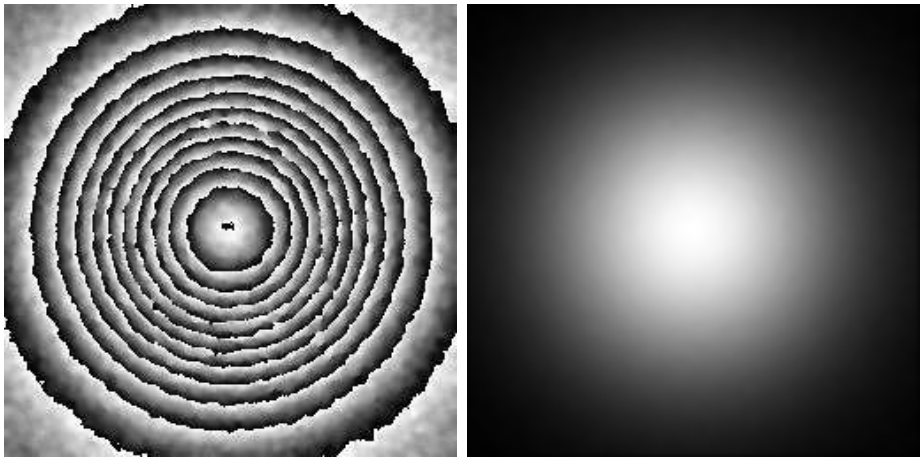

Figure 7.4: Compensated deformation map and its unwrap

Finally, the linear deformation is added to the compensated deformation to obtain the total deformation of the test object, presented in Figure 7.5.

7.3 Composite deformation measurement

The same measurement layout is used as in the previous section, presented in Figure 7.1. The diaphragm is mounted on a rotating stage, which introduces a rotation in addition to the point deformation. The rotating stage has an arm of length $l = 65$ mm positioned by a micrometer screw. One unit of rotation is defined to correspond to $d = 10$ μm displacement

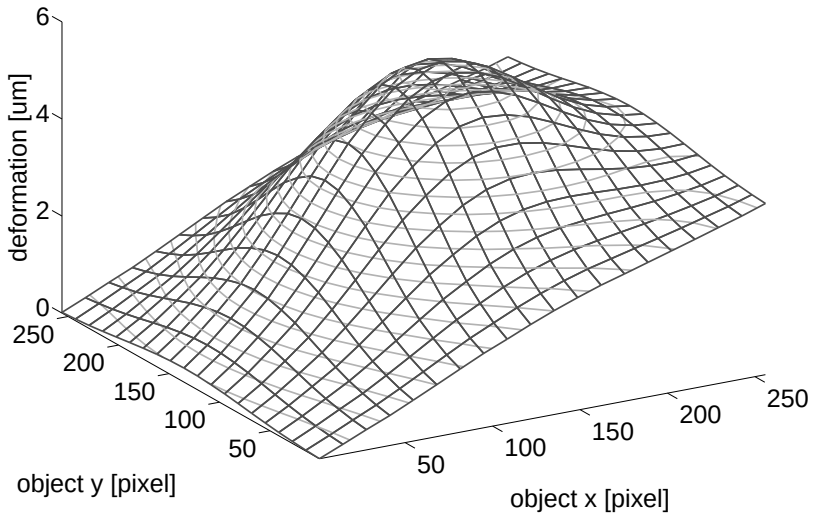

Figure 7.5: Total deformation

of the arm at distance l from the center of rotation, resulting in a rotation of $\Delta\varphi_{\text{unit}} = \frac{d}{l} = 2.44 \cdot 10^{-4}$ rad.

The diaphragm is $a = 40$ mm wide, which appears to be $n = 840$ pixels on the images. The illumination shines on the object at an angle $\theta = 30°$ to surface normal. Hence one unit of rotation causes an x-directional phase gradient of

$$\frac{\partial\phi}{\partial x} = \frac{2\pi}{\lambda}\frac{a\Delta\varphi_{\text{unit}}}{n}(1+\cos\theta) = 0.136\ \frac{\text{rad}}{\text{pixel}} \tag{7.7}$$

according to Equation (3.1). This corresponds to one interference fringe every 46 pixels.

One measurement is presented here, processed in a fashion simiar to the simulation explained above. A rotation of 2.25 units is introduced in addition to the local diaphragm deformation. Figure 7.6 shows the resulting correlation image and phase map.

The phase map is low-pass filtered and unwrapped, see Figure 7.7. 8% of its area cannot be unwrapped because of the too dense interference fringes. Linear fit shows that the average steepness is 0.297 radians/pixel in the x direction and a negligable -0.076 radians/pixel in the y direction. This suggests a rotation of 2.19 units. The calculated phase gradient in the y direction compared to the lack of corresponding rotation provides us with a coarse estimate of the precision of the method. This is due to the random shape of the non-unwrapped region and other artifacts of the unwrapping algorithm described later. However, our goal is not to measure the rotation component exactly, but to have an estimate good enough to unwrap the whole image. It is also possible that the first linear fit and compensation allows unwrapping a larger area but still not the entire image and thus another iteration is needed.

This value is used for compensation of the raw phase map as described in the previous section. The compensated phase map low-pass filtered and finally unwrapped is presented in Figure 7.8. It is clearly seen that the whole image can be unwrapped after compensation.

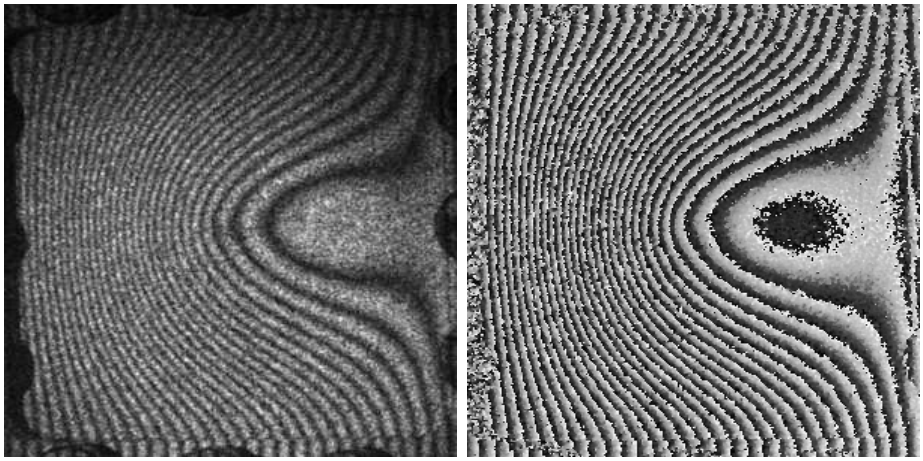

Figure 7.6: Correlation image and deformation map

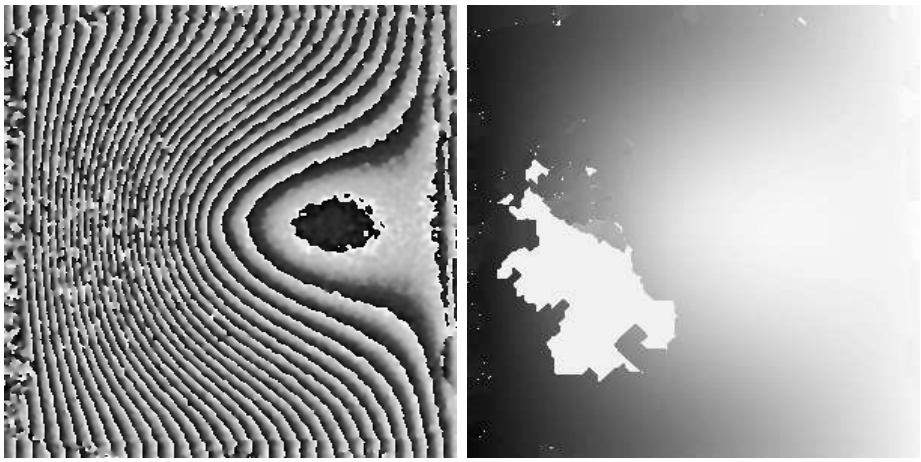

Figure 7.7: Smooth deformation map and its unwrap

The border of the image shows parts of the frame clamping the diaphragm, these areas do not show the deformation of the diaphragm and can be cut when presenting a 3D deformation graph.

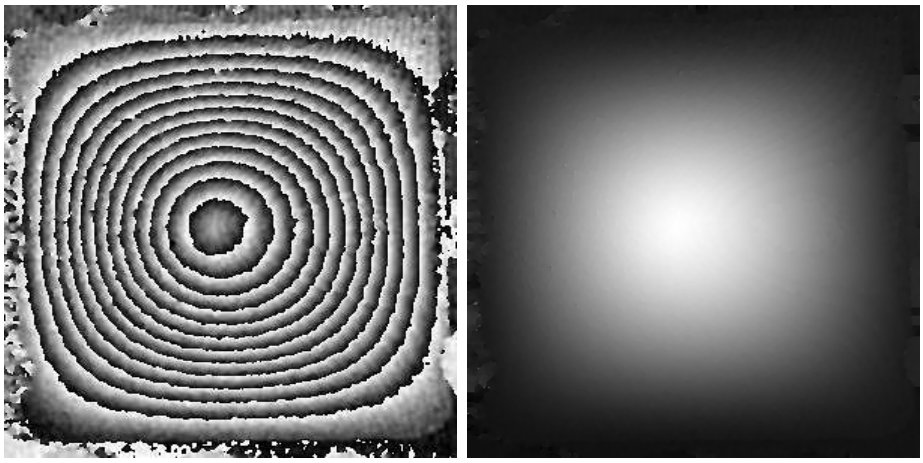

Figure 7.8: Compensated deformation map and its unwrap

As the last step, the linear deformation component used for compensation is added to the compensated deformation map to reconstruct original deformation of the object. This is shown in Figure 7.9.

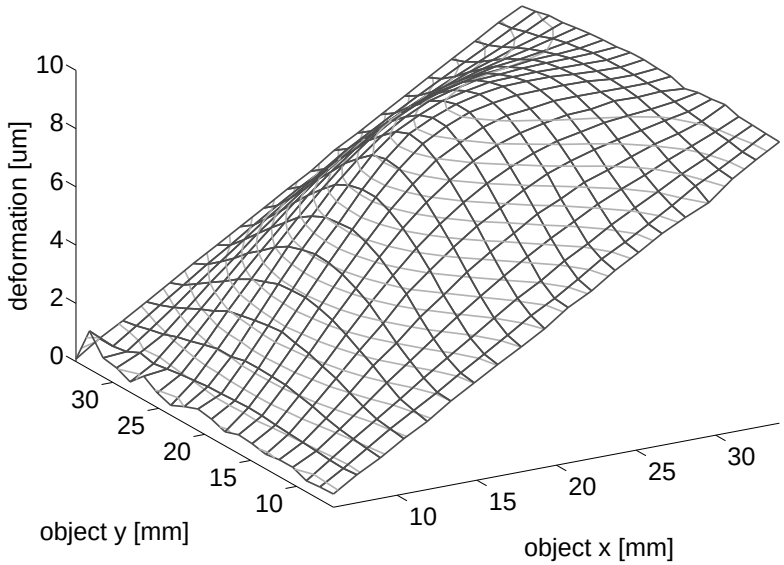

Figure 7.9: Total deformation

7.4 Conclusion

- Deformation components are investigated and classified for our needs.
- A method of carrying out arbitrary linear transformations on 2π-cyclic phase values such as smoothing is presented.
- Linear fit is applied to approximate linear deformation component. This method is also extended to the case where only parts of the deformation map can be unwrapped.
- A scenario is invented where deformation compensation with approximated linear component reduces maximum deformation gradient.
- Specific cases are presented in simulation and measurement as well where this compensation makes deformation processing possible.

We conclude that the idea of deformation component separation comes handy not only for industrial nondestructive testing but also to make it possible to process deformations involving large rotations or other components of low order.

8 Deformation component separation in measurement

A measurement layout is proposed for separating deformation components. Measurements are carried out on this setup.

8.1 Methods of feedback

This section presents how detected deformation components can be used to control measurement circumstances so that they can be separated. At the first stage, camera images are recorded and processed to obtain information about global components, which are then fed to a hardware compensation system moving the test object in such a fashion that these components disappear to reveal the local components in the second stage of measurement. To demonstrate this scheme, rotation along one axis is carried out just like in the previous section. The test object is rotated back manually by the calculated degree of rotation.

Measurement layouts featuring another object as the source of reference wavefront makes compensation possible by means of carrying out the corresponding rotation or other deformation on the reference object. This makes it necessary for the two objects to both be in focus, in other words, to be mirrored images of each other with respect to the beamsplitter uniting their wavefronts to the camera. In this most simple setup it also means that the deformations are mirrored.

Another option is to use a spatial light modulator (SLM) to alter the reference wavefront. An SLM is a transparent matrix of pixels capable of shifting the phase of the light separately at each pixel. This would have to be placed in the mirrored position of the test object in the way of the diffracted wavefront, or in the planar wavefront illumination the reference object. However, as SLM's tend to be small, an additional imaging optics would be needed for an object of the size of ours.

8.2 Calibration

In this experiment, the same experimental setup is used as in the previous section, with the same illumination angle $\theta = 30°$. However, images are captured with different zoom so

that the diaphragm is now $n = 875$ pixels wide. This results in a phase gradient per unit rotation of

$$\frac{\partial\phi}{\partial x} = \frac{2\pi}{\lambda}\frac{a\Delta\varphi_{\text{unit}}}{n}(1+\cos\theta) = 0.130\ \frac{\text{rad}}{\text{pixel}}. \tag{8.8}$$

First the rotation stage is calibrated. Single images are recorded with steps of rotation of quarter units and compared with a set of four phase-shifted images at a position defined as origin. These deformations are then processed and the ones with less then 80% of the image area unwrapped are omitted. The fit of a line shows us that one unit of rotation results in 0.136 radians/pixel in the x-direction phase gradient. The data points and fit are displayed in Figure 8.1.

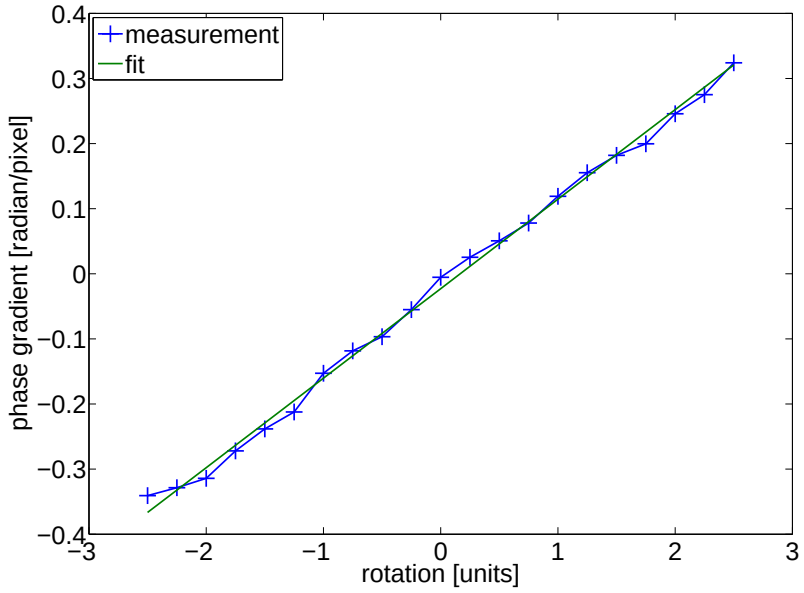

Figure 8.1: Phase gradient versus rotation

8.3 Measurement

Now the diaphragm is deformed locally and rotated by 4.75 units. The recorded images lead to a fairly dense fringe pattern, which only loosens on one side of the deformation. This is the only area where unwrapping is possible. The result is shown in Figure 8.2.

It is important to note about the unwrapped deformation map that it has sharp edges within the allegedly successfully unwrapped area. This comes from the nature of the unwrapping process. Goldstein's branch-cut algorithm operates focusing on the singularities. These singularities are unavoidable to some extent in practice and they make unwrapping a difficult task. The idea is to pair and connect nearby singularities of opposite sign and do the integration avoiding these cuts. However, with so noisy images it might happen that remote singularities get connected, resulting in discountinuities along long curves. Figure 8.3 shows the bottom right area of the unwrapped phasemap magnified to illustrate this situation. This definitely biases the linear fit.

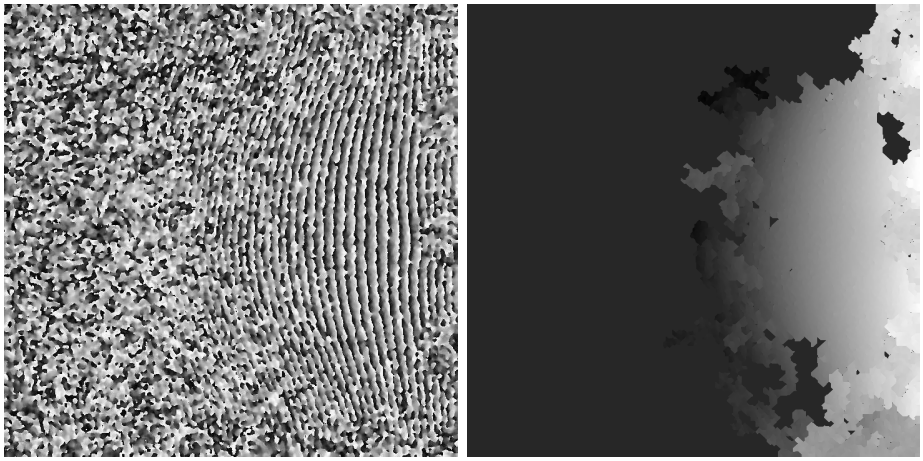

Figure 8.2: Smooth phasemap and its unwrap of the uncompensated deformation

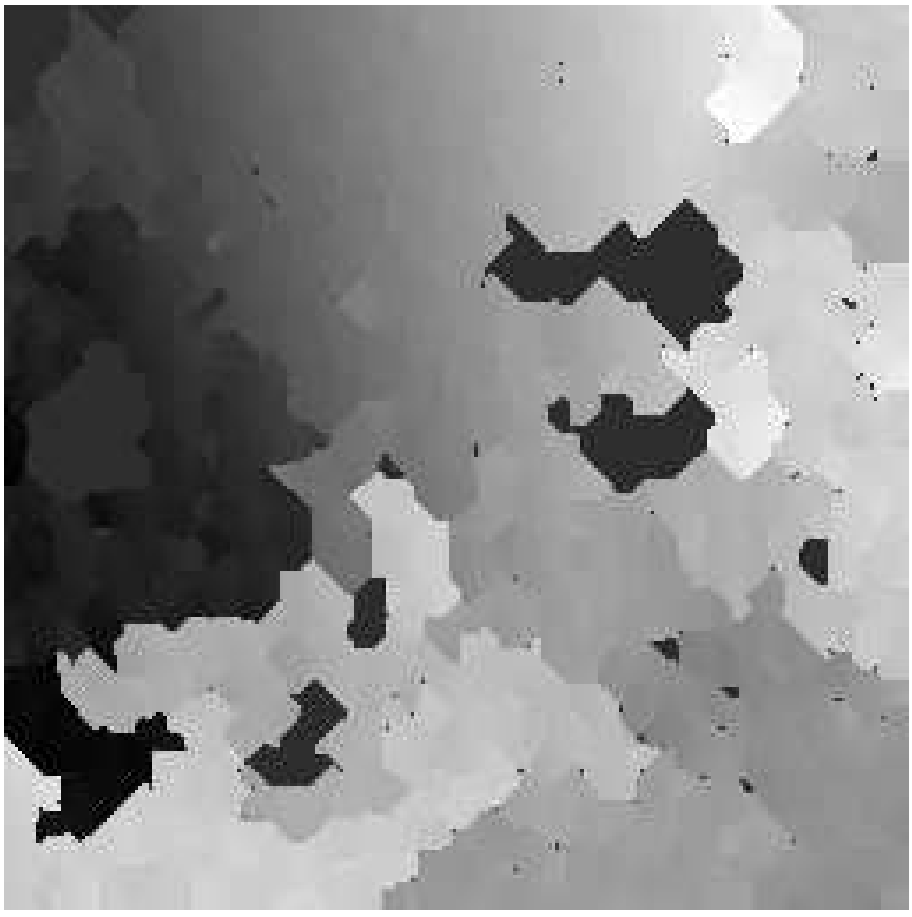

Figure 8.3: Unwrap with discountinuities magnified

Phase gradient is found to be 0.353, corresponding to a rotation of 2.7 units. Note that this is close to the half of the real rotation. This is due to that only a small area of the image could have been unwrapped, exactly where fringes were sparsened, yielding a highly biased result.

Now the rotation stage is manually rotated backwards by 2.75 units to emulate a computer-controlled compensation system. The measured phasemap and deformation are presented in Figure 8.4. The compensation value from the first iteration is so biased that it does not make unwrapping possible after one step. Now another linear fit is carried out to provide the phase gradient of 0.191, corresponding to 1.5 units. Note that the unwrapped area still features the flatter areas with larger weight, resulting in a biased linear fit once again.

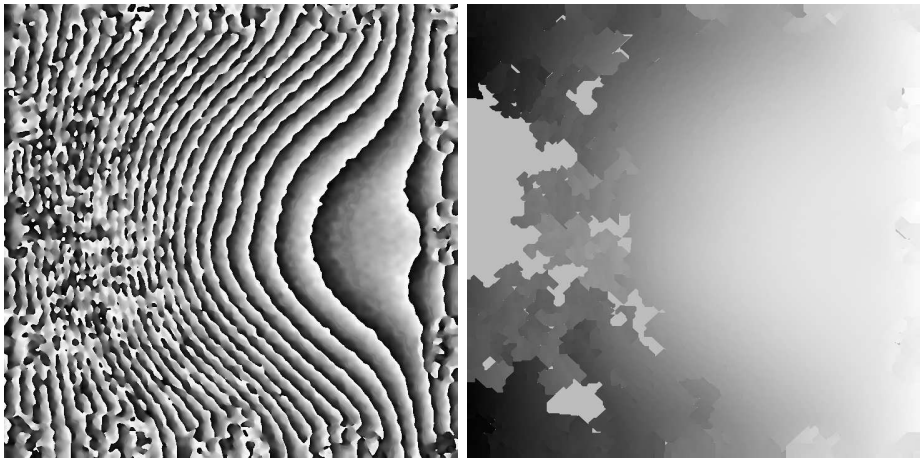

Figure 8.4: Phasemap and unwrap after the first iteration

These add up to a total compensation of 4.25 units versus the real rotation of 4.75. Carrying out this compensation on the test object leads to the phasemap and deformation map presented in Figure 8.5. Though the linear compononent is still not completely eliminated, as 0.5 units of rotation remains, however, this phasemap can at least be unwrapped entirely.

Now as usual, the areas disturbed by the screws or their shadows are cut off and the total deformation is displayed on a 3D graph in Figure 8.6, obtained by adding the total rotation used for compensation to the result of the compensated measurement. Note how much the rotation dominates over the point deformation of the diaphragm.

8.4 Conclusion

- A measurement scheme is presented where partial processing of the recordings leads to compensation parameters that are fed back to the object deformation to obtain recordings possible to process.
- A scenario is presented where two iterations are necessary due to the biased nature of the obtained global deformation component coefficient as the steeper areas are more difficult to unwrap than the flatter ones.

This scheme is highly adaptive to the global deformation of the object and it can be extended to involve other methods of compensation, such as deformation of reference object, deformation via motorized stage or SLM.

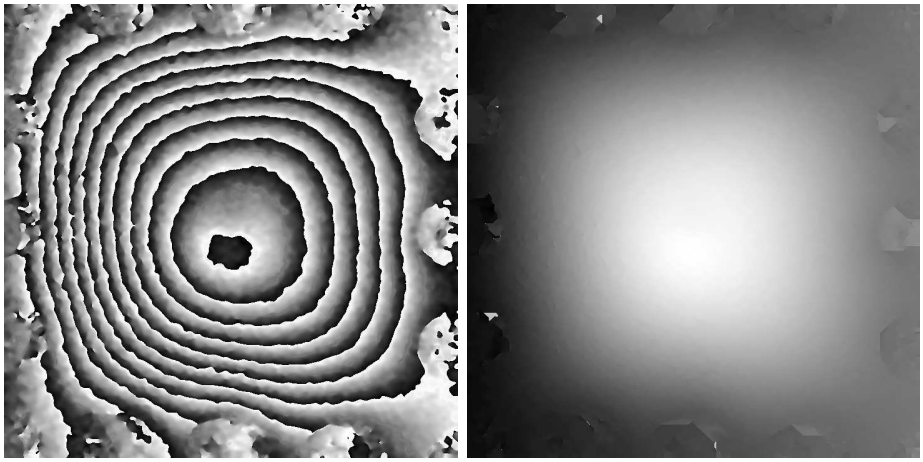

Figure 8.5: Phasemap and unwrap after the second iteration

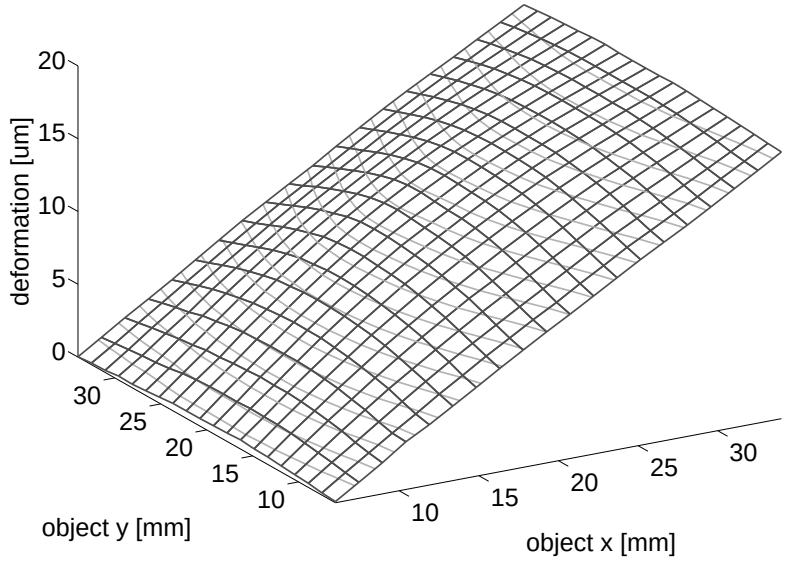

Figure 8.6: Total deformation

9 Large deformations

A measurement procedure is elaborated for large deformations in such a manner that the measurement system is capable of controlling the measurement sensitivity. Its features are presented in simulation and measurement as well.

9.1 Concept

Noise and minimum fringe spacing in pixels determine whether a deformation can be processed or not. The previous two sections deal with a case where deformation gradient can be decreased by means of compensation for rotation. Now deformations requiring more complicated methods are examined. This might be the case of a nearly circular deformation with too large magnitude, resulting in a large area impossible to process. Rotation of the object could only reveal part of this area. However, if we had an idea about the local deformation, for instance, if we knew its approximate center and magnitude, compensation could lead to a completely unwrappable phasemap. In order to obtain this, two measurements with different sensitivities are used on the same object.

A natural question would arise why to use two measurements, if one of them has to be desensitized enough to provide a complete deformation map anyway. The additional measurement has many advantages. One of them is that desensitized speckle arrangements might have unwanted sensitivity to in-plane deformations, and this can be compensated for by a carefully planned other measurement. Another feature is that a desensitized measurement has a proportionally lower precision, so correction by an additional, more sensitive measurement provides a resolution to maximal deformation ratio not achievable by a singe measurement.

In this experimental setup, a desensitized speckle measurement and a digital hologram measurement is implemented. The speckle measurement gives us a coarse deformation map with which the digital hologram can be compensated to make its otherwise indistinguishable interference fringes processable. Interferometric digital holography provides complex values, their argument corresponding to the deformation and magnitude having speckle nature, without taking phase-shifted captures. Therefore deformation compensation can be carried out right away in the form of multiplication by a complex number of unit absolute value. However, to avoid the speckled nature of this phase information, with less intense pixels being more supressed by noise, fringes are formed by substracing reconstructed holograms and low-pass filtering as in ESPI.

9.2 Measurement layout

For digital holography, beams 1 and 2 are used and the imaging optics is removed, see Figure 9.2. For ESPI, beams 2 and 3 are used with the imaging optics, as in Figure 9.2. In practice, four digital hologram recordings are taken, then the imaging optics is inserted on its separate mount, its is adjusted and focused, to take four exposures for speckle interferometry. Then the object is deformed, another speckle recording and finally, after the removal of the imaging optics, a last holograpic image is taken.

The illumination angles are $\theta_2 = 20°$ and $\theta_3 = 55°$, that gives us one interference fringe for 1.72 μm deformation in the desensitized arrangement and one fringe for 0.326 μm deformation in the holographic arrangement, where only illumination at angle θ_3 is used. This provides a ratio of 5.30 between the two measurements. See Equations (3.1) and (3.3) for further explanation.

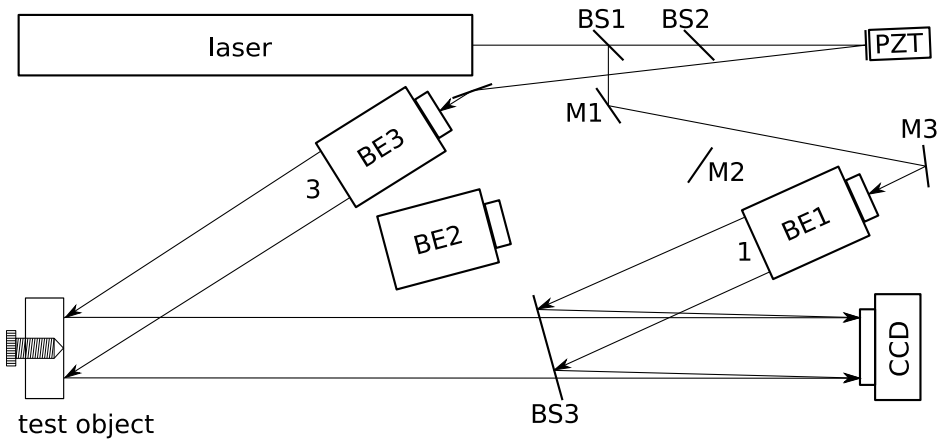

Figure 9.1: Measurement setup for digital holography
Beamsplitter BS1 divides reference beam and object illumination beam. Beam expander BE1 provides planar reference wavefront 1 and BE3 illuminates object with phase shifted beam 3. Beamsplitter BS3 merges object and planar reference wavefront.

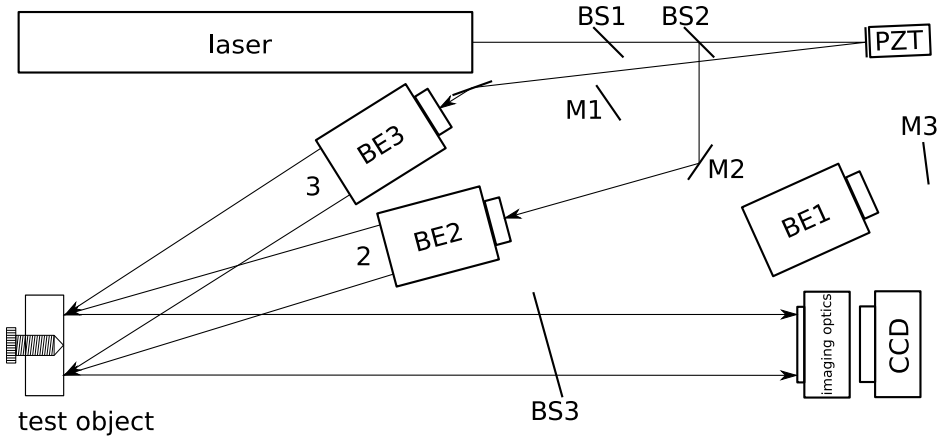

Figure 9.2: Measurement setup for ESPI
Beamsplitter BS2 splits beam into beam expanders BE2 and BE3, illuminating the object with beams 2 and 3.

9.3 Measurement results

Two measurements are presented here. In both cases, a maximum deformation of 11.75 μm is achieved with the micrometer screw. In case A, all 16 screws are tightened, holding the diaphragm uniformly. This results in a mostly circular deformation. In case B, six screws are removed to provide a deformation of less regular shape.

To align the hologram and ESPI measurements, a square is cut out from both, determined by the center of the screws. This region is shown on all the images in this section. This square is not selected with high presicion, however, the compensation technique is quite tolerant to small misalignments.

Figure 9.3 presents the wrapped deformation maps obtained by the desensitized speckle measurement. It shows clearly the amplitude and the shape of the deformations. It can also be seen that there is no useful data in the dark areas of the image, that is, on the surface of the black screws and on the right side where they cast shadow on the diaphragm.

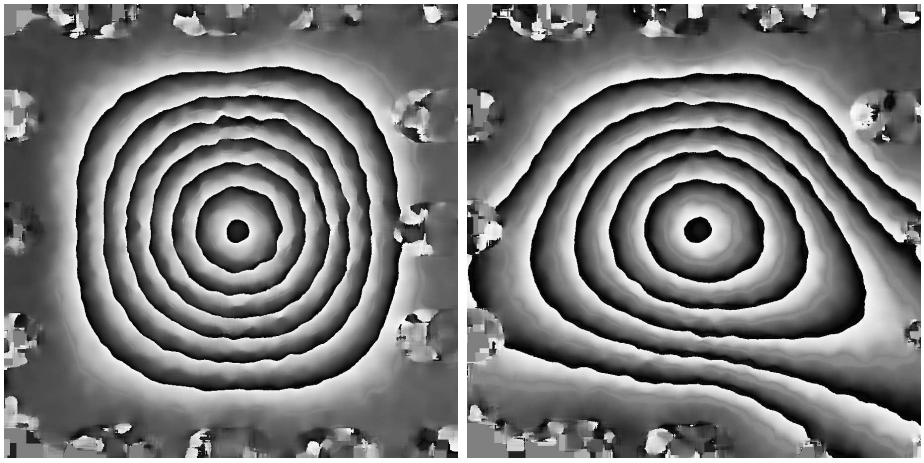

Figure 9.3: Desensitized ESPI deformation maps

Five digital holograms are reconstructed for each case. These carry complex information about the wavefront reflected from the object. If the difference of the holograms before and after deformations are formed, the resulting complex values will feature interference fringes in their amplitude. To compensate with the result of the speckle measurement, one of the complex terms is to be rotated by the corresponding angle pixelwise.

The four holographic interference fringe patterns are then fed into Carré's method to result in a deformation phasemap. Figure 9.4 shows the phasemap in case no compensation is applied. It is clearly seen that these phasemaps have wraps so tightly spaced that it is impossible to unwrap them.

Figure 9.5 presents the phasemap from the compensated holographic interference images. A compensation with coefficient 5.3 is carried out. This value is not only given by the measurement angles, but it is found to be optimal via manual trial-end-error. These phasemaps can now easily be unwrapped. Experimenting with the phasemaps shows that different compensation coefficient is also enough to sparse the finges to a processable extent, thus no a priori knowledge of the exact ratio of measurement sensitivities is needed. Also note that as Goldstein's method is implemented with feedback about the unwrapped area, it is easy to elaborate an algorithm experimenting with compensation coefficients in a wide range to

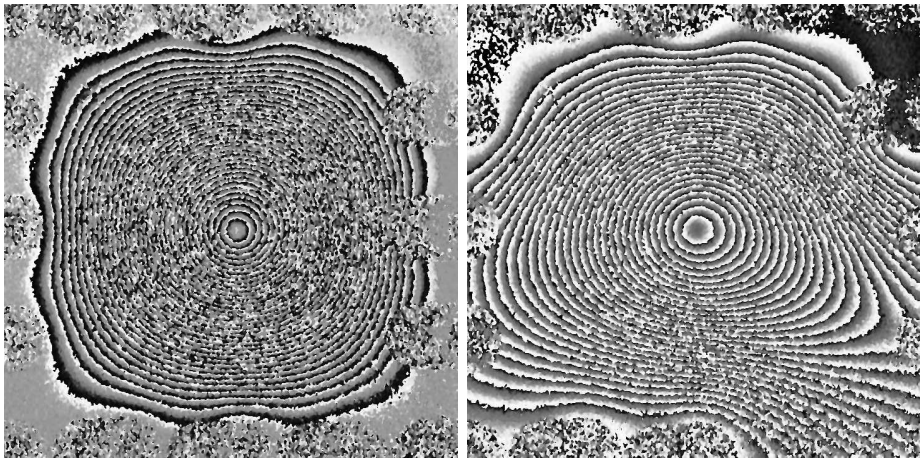

Figure 9.4: Interferometric hologram phasemaps without compensation

adaptively find the best value, even if no a priori knowledge is present at all about the ratio of sensitivities.

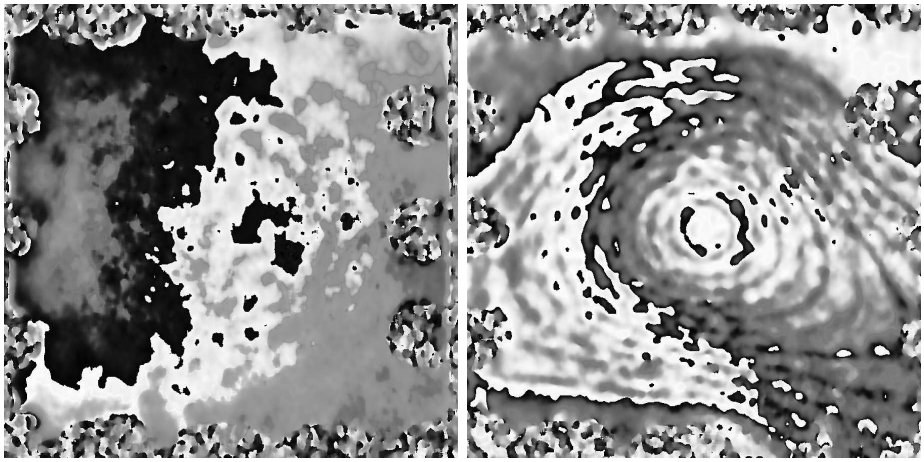

Figure 9.5: Interferometric hologram phasemaps with compensation: 5.3

Figure 9.6 presents a case when only a compensation of 4.9 is used, so a few phase jumps are still present. Note that they are already sparse enough to be unwrapped.

The compensated phasemaps using the coefficient of 5.3 are unwrapped and then the compensation is added to the result to obtain the total deformation. Finally, the areas corresponding to the screws are clipped to end up with the deformation of the visible diaphragm area. These are shown in Figures 9.7 and 9.8.

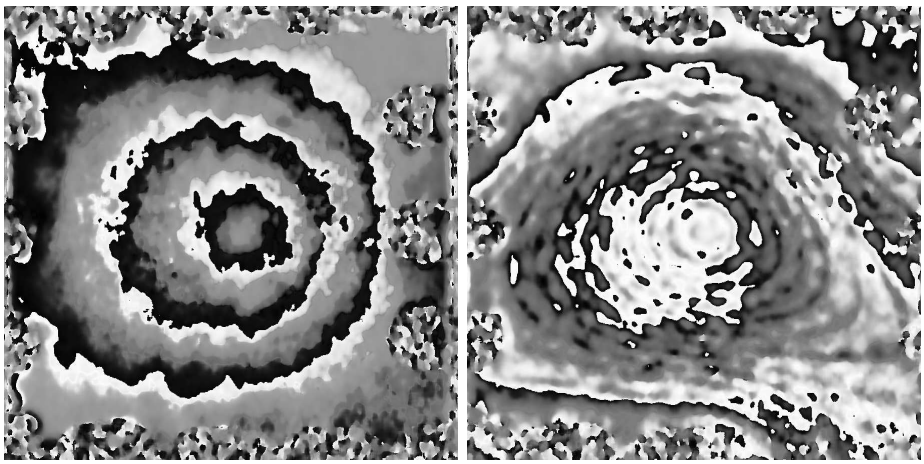

Figure 9.6: Interferometric hologram phasemaps with undercompensation: 4.9

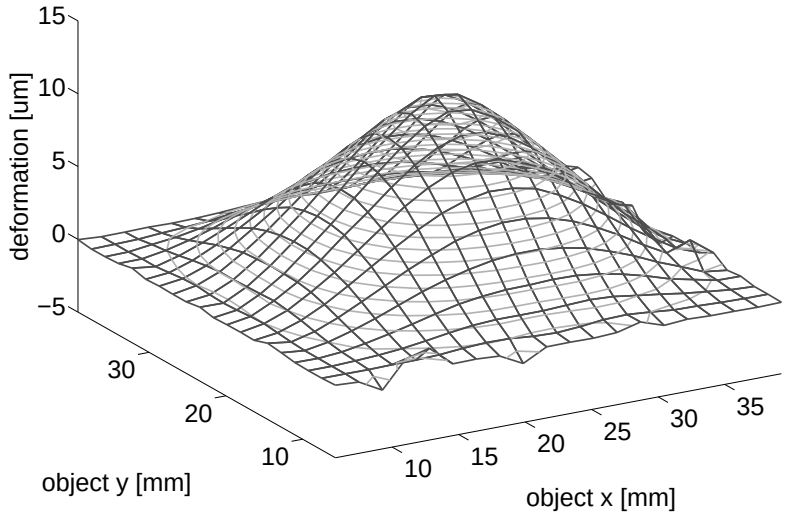

Figure 9.7: Total deformation in case A

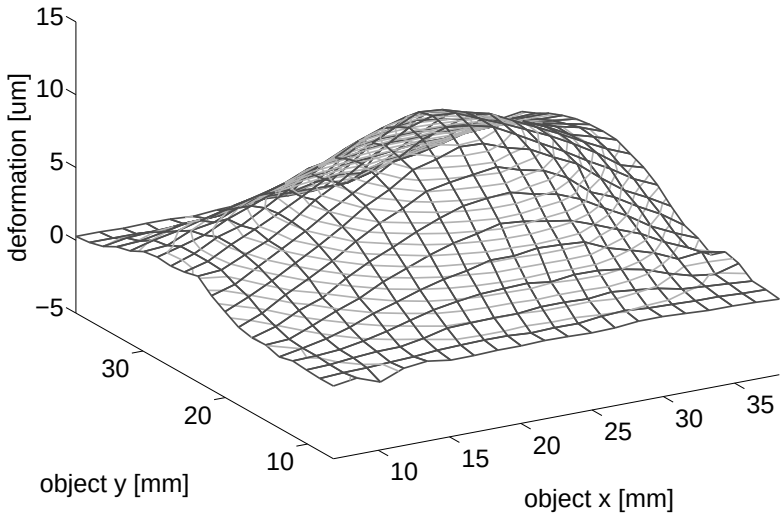

Figure 9.8: Total deformation in case B

9.4 Conclusion

- Too tightly spaced interference fringes have been resolved by means of compensation by another measurement of lower sensitivity and different nature. This way combining an ESPI and a digital holographic interferometric measurement has been demonstrated.
- It has been investigated that compensation leads to processable results even if the measurement ratio is not known exactly or there is a small spatial misalignment in the two maps.

Note that two desensitized ESPI measurements can also be combined in a similar fashion, no specific feature of digital holography is made use of. Taking only one holographic capture, that is, without phase shift, and using phase values obtained from that could have been a simplification which cannot be carried out if both measurements were ESPI. However, an advantage would be that images of the object on the captures do not have to be adjusted if using a double ESPI setup.

A further improvement is to control illumination angles by computer to change measurement sensitivities. If both arrangements are ESPI, the test object can be mounted on a rotating stage to change the three illumination angles, keeping their difference. It has already been noted that observation angle does not influence desensitized arrangements. If beam expanders are fed via glass fibers, they can be separately aligned to provide desensitization factors over a greater range.

It is mainly the size of the beam expanders determining the minimum angle difference and the object surface with occasional humps casting shadows at large illumination angles that limit the range of desensitization.

10 Quality measures

Quality measures are proposed as an aid for the processing and analysis of interference images.

Metrology consists of not only obtaining the value of a quantity by means of measurement, but also to have an indicator on its certainty and reliability. Apart from the precision to which wavelength, illumination and observation angle and other physical parameters of the arrangement are known, it is also essential to evaluate the certainty with which fringes can be identified and bright and dark areas in either an interference pattern or a correlation image distinguished.

Fringes are of speckled nature in coherent measurements, and this would render interpretation of phase values difficult since noise dominates in dark areas between speckles. Therefore it is always the next step to average over them once a correlation image is formed. Also speckle intensity distribution is given within the circumstances of our experiments, that is, surface roughness and optical path differences from a given point of the object to one of the camera CCD much larger than wavelength. Hence no quality measures need to be introduced concerning the speckled image, only the low-pass filtered fringe pattern is to be evaluated.

Traditionally fringe visibility is used to quantify how characteristic fringes are. This requires an area small enough to correspond to uniform illumination of the test and reference objects, however, large enough to feature a fringe maximum and a fringe minimum. Then it is defined as

$$V = \frac{I_{\max} - I_{\min}}{I_{\max} + I_{\min}}. \tag{10.9}$$

It is clear that this value ranges in $[0, 1]$, being 0 iff $I_{\max} = I_{\min} \neq 0$, that is, on a constant image, and being 1 iff $I_{\max} \neq I_{\min} = 0$, that is, the darkes areas are of zero amplitude. [16]

This visibility measure however fails in case no such area is available, particularity when there is no π difference in total or if illumination is too uneven. Even if such an area exists, it requires further investigation to find one, involving separation of overall illumination from fringe pattern, which is much more complex than the original task.

To avoid the problem of selection of a suitable area in case of uneven illumination, phase shift is taken advantage of and a local quality measure is introduced. Local refers to that only the four values corresponding to the same pixel of the correlation images are considered.

To invent this measure, first it is to note that in case one of the interfering wavefronts has an amplitude saturating the camera, the resulting pixel is going to be of little information content. Here at least two of the four values are going to be saturated in case phase shift is close to $\frac{\pi}{2}$. If this amplitude is much higher than the other, then all values are saturated.

Similarily, the average of an area consisting of most but not all of saturated pixels, will result in pixel values close to each other, and parallely, unreliable phase values.

Also if one of the amplitudes is small compared to noise, the resulting phase is going to be unreliable. This also means that the four values are going to be close to each other, compared to unavoidable noise level.

On the other hand, if there is no saturation and both amplitudes are high enough compared to noise, the four pixel values have a greater variance and in the meanwhile, the result is quite reliable. This leads to the idea of using the variance, or equivalently, its square root, the standard deviation.

Now this quality measure can be used to select the best illumination setup among a few for each pixel separately, as seen in Section 6. The numerous successful experiments presented justify the selection of variance as quality measure.

This quality measure, with an appropriately selected treshold with respect to noise, can be applied to conduct a series of captures with different illuminations, selected and controlled purely by computer, in such a manner that all image areas are explored with satisfactory reliability.

11 Conclusion

Two adaptive methods towards object reflection and illumination have been presented and studied. They cover the most natural ideas for this task. The method of merging results from separately processed captures is found to be efficient and reliable enough to be widely used. Note that dynamic range extension is a method with more strict conditions on the captures and thus on the test object or measurement layout, however, if a measurement can be processed with this method then it can also be processed separately and then merged.

Possible deformation components are investigated and classified. Many examples are presented to show that low order global deformation components can be approximated and substracted from total deformation, and that this can be done either logically, as part of the processing of the results, or by a feedback to the measurement system. It is also proven by examples that this method might lead to working results in cases where regular processing does not work. That is, this method is capable of extending measurement range.

For large deformations, a composite method is presented. Two measurements of different sensitivity are carried out and combined to take advantage of the higher measurement range of one and the larger precision of the other. It is investigated that this combination of measurements is robust to small spatial misalignments and not exact desensitization ratios. The measurement two be combined can be of different natures, ESPI or digital holograpy. In case of ESPI, measurement sensitivity can easily be adjusted by changing illumination angles.

References

[1] J. A. Leendertz: Interferometric displacement measurement on scattering surfaces using the speckle effect. Journal of Physics E: Scientific Instruments. 1970, volume 3, issue 3, pp. 214–218.

[2] Attila Németh, János Kornis, Zoltán Füzessy: Fringe compensation measurement in holographic interferometry using phase-shifted interferograms. Optical Engineering, 2000, volume 39, issue 12, pp. 3196–3200.

[3] Ole J. Løkberg, Gudmunn Å. Slettemoen: Interferometric comparison of displacements by electronic speckle pattern interferometry. Applied Optics, 1981, volume 20, issue 15, pp. 2630–2634.

[4] Pramod K. Rastogi, Pierre Jacquot: Measurement of difference deformation using speckle interferometry. Optics Letters Volume, 1987, volume 12, issue 8, pp. 596–598.

[5] Charles J. Joenathan, A. R. Ganesan, Rajpal Singh Sirohi: Fringe compensation in speckle interferometry: application to nondestructive testing. Applied Optics, 1986, volume 25, issue 20, pp. 3781–3784.

[6] A. R. Ganesan, Charles J. Joenathan, Rajpal Singh Sirohi: Real-time comparative digital speckle pattern interferometry. Optics Communications, 1987, volume 64, issue 6, pp. 501–506.

[7] Øystein Skotheim: Holovision. Diploma thesis. Trondheim, 2002.

[8] Atsushi Wada, Takeshi Kurashima, Yoko Miyamoto, Mitsuo Takeda: Reconstruction of phase-shift digital holograms with unknown phase-shift by fourier fringe analysis. Proceedings of SPIE, 2003, volume 5144, pp. 138–141.

[9] Richard M. Goldstein, Howard A. Zebker, Charles L. Werner: Satellite Radar Interferometry: Two-dimensional Phase Unwrapping. Radio Science, 1988, volume 23, issue 4, pp. 713–720.

[10] Malgorzata Kujawiñska: Adaptivity: Problem or Solution? Fringe 1997 Conference Proceedings, pp. 419-431.

[11] János Kornis, Zoltán Füzessy, Attila Németh: Adaptive systems in speckle-pattern interferometry. Applied Optics, 2000, volume 39, issue 16, pp. 2620–2627.

[12] Ichirou Yamaguchi, Ji-yuan Liu, Jun-ichi Kato: Active phase-shifting interferometers for shape and deformation measurements. Optical Engineering, 1996, volume 35, issue 10, pp. 2930–2937.

[13] Eduardo A. Barbosa, Jaime Frejlich, Viktor V. Prokofiev, N. J. Gallo, Jose P. Andreeta: Adaptive holographic interferometry for two-dimensional vibrational mode display. Optical Engineering, 1994, volume 33, issue 8, pp. 2659–2662.

[14] Jaime Frejlich, A. A. Kamshilin, V. V. Kulikov, E. V. Mokrushina: Adaptive Holographic Interferometry Using Photorefractive Crystals. Optical Communications, 1989, volume 70, pp. 82–86.

[15] Zoltán Füzessy, János Kornis, Attila Németh: Fringe pattern compensation by synthesis of phase-shifted interferograms. Proceedings of SPIE, volume 4398, pp. 35–44.

[16] Robert Jones, Catherine Wykes: Holographic and Speckle Interferometry. Cambridge University Press, 1983.

[17] Ulf Schnars, Werner Jueptner: Digital Holography. Springer-Verlag 2005.

[18] Kjell J. Gåsvik: Optical Metrology. John Wiley & Sons, 1995.

[19] `http://www.cv.tu-berlin.de/rat/forum/viewtopic.php?t=37&sid=ddcd959cce778ca7b29153f10ef88028`